Splitting of the isovector giant dipole resonance in neutron-rich spherical nuclei

V. M. Kolomietz,[1,2] A. G. Magner,[1] and S. Shlomo[2]
[1]*Institute for Nuclear Research, Prosp. Nauky 47, 03680 Kyiv, Ukraine*
[2]*Cyclotron Institute, Texas A&M University, College Station, Texas 77643, USA*
(Received 26 May 2005; published 17 February 2006)

The well-known splitting of the isovector giant dipole resonance is traditionally explained as a phenomenon of the nuclear isospin asymmetry (isospin splitting model) or the nuclear deformation. We suggest a new mechanism of the splitting of the giant multipole resonances in spherical neutron-rich nuclei resulting from the interplay of the isovector and isoscalar sounds with different velocities. Our approach is based on the collisional Landau kinetic theory and can be used for description of the splitting phenomena for both the isoscalar and the isovector modes in a wide region of nuclear masses $A \sim 40$–240. For the isovector dipole modes, the evaluated values of the splitting energy, the relative strength of the main and satellite resonance peaks, and the contribution to the energy-weighted sum rule are in agreement with experimental data.

DOI: 10.1103/PhysRevC.73.024312 PACS number(s): 24.10.Cn, 21.60.Ev, 24.10.Nz, 24.30.Cz

I. INTRODUCTION

The splitting of the isovector giant dipole resonance (IVGDR), which is observed in the isospin conjugate photonuclear (γ, n) and (γ, p) reactions, is often explained as a phenomenon of the nuclear isospin asymmetry within the isospin splitting model (ISM). The ISM assumes that both the main peak and the satellite correspond, respectively, to the two different isospins $T_0 + 1$ and T_0, where $T_0 = T_3 = (N - Z)/2 \neq 0$ is the isospin of the ground state of the asymmetric nucleus [1–12]. In heavy nuclei, the (γ, p) cross section approximately corresponds to the $T_0 + 1$ component of the IVGDR whereas the (γ, n) cross section corresponds to its T_0 component. These two component are separated in energy by [13,14]

$$\Delta E = E_{T_0+1} - E_{T_0} \approx \overline{b}_{\rm sym} \cdot X, \tag{1}$$

where $\overline{b}_{\rm sym} = b_{\rm sym}(T_0 + 1)/T_0$ is the symmetry energy for the dipole mode, $b_{\rm sym} \approx 30$ MeV is the isotopic symmetry energy, $X = (N - Z)/A$ is the asymmetry parameter, and A is the mass number of the nucleus.

Another IVGDR splitting caused by deformations of the nucleus was intensively studied in photonuclear and electronic inelastic scattering reactions (see Refs. [6,7,12,15]). It can be explained within macroscopic models [16]. In this case, the energy splitting ΔE between two components, $E_{\rm high}$ and $E_{\rm low}$, of the IVGDR is proportional to the deformation $\delta = \Delta R/R$ of the nucleus (with ΔR the difference between the curvature radii parallel and perpendicular to the symmetry axis and R the nuclear mean radius) [17]:

$$\Delta E = E_{\rm high} - E_{\rm low} \approx \overline{b}_{\rm def} \cdot \delta, \tag{2}$$

where $\overline{b}_{\rm def}$ is the mean IVGDR energy.

However, experimental data [2–12] indicate that the splitting of the isovector giant resonances into two or more peaks is a more general effect than the one obtained in the conjugate (γ, n) and (γ, p) reactions or in deformed nuclei. For instance, in many almost *spherical* (neutron-rich and heavy enough) nuclei such as several Ca, Ni, and Sn isotopes, one can observe the splitting of the IVGDR. Theoretically, the isotopic asymmetry features of giant multipole resonance structure and the coupling between the isoscalar and isovector modes in neutron-rich nuclei were studied in Refs. [18–20] within the microscopic Hartree-Fock (HF) based random phase approximation (RPA).

In the present paper we suggest a quite general explanation of the splitting of both the isoscalar and the isovector modes in spherical neutron-rich nuclei within the Fermi-liquid-drop model (FLDM) [21–23], based on Landau kinetic theory [24], which was extended to two-component asymmetric nuclei [25]. We point out the importance of the excitation of two sounds with slightly different velocities in the finite asymmetric Fermi liquid as a reason for such splitting. This mechanism of energy splitting is essentially different from the ISM of Eq. (1). In contrast to the ISM, we discuss the two-peak structure (main peak and its satellite) of the IVGDR for each reaction (γ, n) and (γ, p) independently rather than comparing the main peaks from both isospin conjugate reactions (γ, n) and (γ, p), as done in the case of ISM [7]. In our approach, the main peak of the IVGDR and its satellite belong to different branches (isovector-like and isoscalar-like, respectively) of the sound mode in an asymmetric nuclear Fermi liquid.

The plan of the paper is the following. In Sec. II we start from the collisional kinetic equation and derive the basic equations of motion for the asymmetric Fermi-liquid drop. The splitting of the giant multipole resonances, which is due to the isotopic asymmetry effect on the dispersion and secular relations, is also discussed in Sec. II. We then derive in Sec. III the response functions for multipole vibrations in the presence of isotopic mixing. The discussion of numerical results is presented in Sec. IV. Our conclusions are given in Sec. V.

II. ASYMMETRIC NUCLEAR FERMI-LIQUID-DROP MODEL

A. Equations of motion in the nuclear volume

In the nuclear volume, where space variations of the equilibrium particle density $\rho_{\rm eq}(\mathbf{r})$ are small, the quasiparticle concept of Landau's Fermi-liquid theory can be applied.

The corresponding collisional Landau-Vlasov kinetic equation (LVKE) for the distribution function $f_q(\mathbf{r}, \mathbf{p}, t)$ of the two-component Fermi liquid ($q = p$ for proton and $q = n$ for neutron) takes the following form [21,22]:

$$\frac{\partial}{\partial t}\delta f_q + \frac{\mathbf{p}}{m_q^*}\nabla_{\mathbf{r}}\delta f_q - \nabla_r(\delta V_q + V_{\mathrm{ext},q})\cdot\nabla_{\mathbf{p}} f_{\mathrm{eq},q} = \delta \mathrm{St}_q[f_p, f_n]. \tag{3}$$

Here $\delta f_q = f_q - f_{\mathrm{eq},q}$ is the variation of the distribution function f_q and $f_{\mathrm{eq},q}$ is the equilibrium Fermi distribution, Eq. (A3); δV_q is the variation of the self-consistent mean field and m_q^* is the effective nucleonic mass. The external field $V_{\mathrm{ext},q}$ will be specified later in Sec. IV and the collision integral $\delta \mathrm{St}_q[f_p, f_n]$ is discussed in Appendix A.

A variation, δV_q, of the self-consistent mean field is given by [24]

$$\delta V_q = \frac{1}{\mathcal{N}_q}\int \frac{2d\mathbf{p}'}{(2\pi\hbar)^3} F_{qq'}(\mathbf{p}, \mathbf{p}')\,\delta f_{q'}(\mathbf{r}, \mathbf{p}'; t), \tag{4}$$

where

$$\mathcal{N}_q = -\int \frac{2d\mathbf{p}}{(2\pi\hbar)^3}\frac{\partial f_{\mathrm{eq},q}(\epsilon_p)}{\partial \epsilon_p} \tag{5}$$

is the averaged density of states. The interaction amplitude $F_{qq'}(\mathbf{p}, \mathbf{p}')$ is usually parametrized in terms of the Landau constants F_ℓ as

$$F_{qq'}(\mathbf{p}, \mathbf{p}') = \sum_{\ell=0}^{\infty} F_{\ell,qq'}\, P_\ell(\hat{\mathbf{p}}\cdot\hat{\mathbf{p}}'), \qquad \hat{\mathbf{p}} = \mathbf{p}/p. \tag{6}$$

For simplicity we will assume

$$F_{\ell=0,qq'} \neq 0, \quad F_{\ell=1,qq'} \neq 0, \quad F_{\ell\geqslant 2,qq'} = 0 \quad \text{and} \quad F_{\ell,pp} = F_{\ell,nn}, \quad F_{\ell,pn} = F_{\ell,np}. \tag{7}$$

We will start from the eigenmotion problem by assuming $V_{\mathrm{ext},q} = 0$ in Eq. (3). In the nuclear interior, the eigensolution (homogeneous solution) $\delta f_{\mathrm{hom},q}(\mathbf{r}, \mathbf{p}, t)$ to Eq. (3) is then given by a superposition of plane waves as

$$\delta f_{\mathrm{hom},q}(\mathbf{r}, \mathbf{p}, t) = \delta(\epsilon_p - \epsilon_{F0,q})\int d\Omega_k \times A_q(\hat{\mathbf{p}}\cdot\hat{\mathbf{k}})\exp[i(\mathbf{k}\cdot\mathbf{r} - \omega t)], \tag{8}$$

where $\epsilon_{F0,q} = p_{F,q}^2/2m_q^*$ is the Fermi energy, $p_{F,q}$ is the Fermi momentum, and

$$A_q(\hat{\mathbf{p}}\cdot\hat{\mathbf{k}}) = \sum_l \nu_{l,q}(\omega, k) Y_{l0}(\hat{\mathbf{p}}\cdot\hat{\mathbf{k}}), \qquad \hat{\mathbf{k}} = \mathbf{k}/k. \tag{9}$$

Here $\nu_{l,q}(\omega, k)$ is the unknown amplitude and l is the multipolarity of the Fermi surface distortion. The zeroth and first $\mathbf{p}$ moments of $\delta f_q(\mathbf{r}, \mathbf{p}, t)$ determine the particle density variation $\delta\rho_q(\mathbf{r}, t)$ and the velocity field $\mathbf{u}_q(\mathbf{r}, t)$, respectively. Namely,

$$\delta\rho_q(\mathbf{r}, t) = \int \frac{2d\mathbf{p}}{(2\pi\hbar)^3}\delta f_q(\mathbf{r}, \mathbf{p}, t), \qquad \mathbf{u}_q(\mathbf{r}, t) = \frac{1}{\rho_{\mathrm{eq},q}(\mathbf{r})}\int \frac{2d\mathbf{p}}{(2\pi\hbar)^3}\frac{\mathbf{p}}{m_q}\delta f_q(\mathbf{r}, \mathbf{p}, t). \tag{10}$$

Using Eq. (8), one can reduce $\delta\rho_q(\mathbf{r}, t)$ and $\mathbf{u}_q(\mathbf{r}, t)$ for a certain value of the multipolarity L of eigenvibrations to the following form (see also Refs. [21–23]):

$$\begin{Bmatrix}\delta\rho_q \\ \mathbf{u}_q\end{Bmatrix} = \begin{Bmatrix} 3i^L m_q^*\rho_{\mathrm{eq},q}/p_{F,q}^2 \\ (3i^{L-1}s_q/kp_{F,q})\nabla_{\mathbf{r}}\end{Bmatrix}\Phi_q\, j_L(kr)Y_{L0}(\hat{r})e^{-i\omega t}, \tag{11}$$

where,

$$s_q = \omega/v_{F,q}k \tag{12}$$

is the dimensionless sound velocity in units of the Fermi velocity $v_{F,q} = p_{F,q}/m_q^*$, $j_L(x)$ is the spherical Bessel function, and Φ_q is the $\mathbf{r}$-independent amplitude. We also introduce the pressure tensor

$$\delta P_{\nu\mu,q} = 2\int \frac{d\mathbf{p}}{(2\pi\hbar)^3}\frac{p_\nu p_\mu}{m_q^*}\delta f_q(\mathbf{r}, \mathbf{p}, t). \tag{13}$$

For the following derivations we will also need the radial components $\delta P_{rr,q}$ of the tensor,

$$\delta P_{rr,q} = \frac{3}{2}\rho_{\mathrm{eq},q}\Phi_q\Big[\left(1 - 3s_q^2 + Q_1^{-1}(s_q)\right)j_L''(kr) + \left(1 - s_q^2 + \frac{1}{3}Q_1^{-1}(s_q)\right)j_L(kr)\Big]Y_{L0}(\hat{r})e^{-i\omega t}, \tag{14}$$

where $Q_1(z)$ is the Legendre function of the second kind and the prime means the derivative of the Bessel function $j_L(x)$. The local quantities $\delta\rho_q$, $\mathbf{u}_q$, and $\delta P_{\nu\mu,\,q}$ are related to each other by the continuity and momentum conservation equations as follows from Eq. (3):

$$\frac{\partial}{\partial t}\delta\rho_q + \rho_{\mathrm{eq},q}\nabla\mathbf{u}_q = 0, \qquad m_q\,\rho_{\mathrm{eq},q}\frac{\partial}{\partial t}u_{\nu,q} = -\nabla_\mu\delta\Pi_{\nu\mu,q}, \tag{15}$$

where $\delta\Pi_{\nu\mu,q}$ is the momentum flux tensor,

$$\delta\Pi_{\nu\mu,q} = \delta P_{\nu\mu,q} + \rho_q\delta V_q\delta_{\nu\mu}, \tag{16}$$

and we have omitted in Eq. (15) the index $\mathbf{r}$ of the vector $\nabla_{\mathbf{r}}$.

B. Dispersion relations

The dispersion relations for the isoscalar and isovector sound modes can be directly derived from the kinetic equation (3). Let us introduce the Landau interaction constants $F_\ell = \left(F_{\ell,\,pp} + F_{\ell,\,pn}\right)/2$ and $F_\ell' = \left(F_{\ell,\,pp} - F_{\ell,\,pn}\right)/2$ in the isoscalar and isovector channels, respectively. In the following we will assume $F_1' = 0$ and $m_p^* = m_n^* = m^* = m(1 + F_1/3)$. Note that we take into account that $m^* \neq m$, owing to the parameter $F_1 \neq 0$, but neglect the difference between the neutron and proton effective masses. This difference (isovector effective mass correction) leads to second-order terms in the asymmetry parameter X (see Eq. (12.14) of Ref. [26]), which are beyond the linear approach considered here. Furthermore, to emphasize our main idea we will neglect temporarily the contribution from the collision integral by taking $\delta \mathrm{St}_q[f_p, f_n] = 0$. (Note that the collision integral $\delta \mathrm{St}_q[f_p, f_n]$ given by Eq. (A11) will be taken into account in our numerical calculations in Sec. IV.) Substituting then

Eq. (8) into Eq. (3) one obtains

$$v_q(\cos\theta - s_q) + \frac{1}{4\pi}\cos\theta\,\Phi_q = 0, \qquad \cos\theta = \hat{\mathbf{p}}\cdot\hat{\mathbf{k}}, \quad (17)$$

with

$$\Phi_q = \frac{1}{2}\left[F_{qp}(1-\Delta)\int d\Omega_{\mathbf{p}}\nu_p + F_{qn}(1+\Delta)\int d\Omega_{\mathbf{p}}\nu_n\right]. \quad (18)$$

Here we have taken into account the isotopic dependence of the Fermi energy (see Refs. [27,28] and Appendix B),

$$\epsilon_{F,p} = \epsilon_F(1-\Delta), \quad \epsilon_{F,n} = \epsilon_F(1+\Delta), \quad \Delta = \tfrac{4}{3}(1+F_0')X, \quad (19)$$

where $\epsilon_F = p_F^2/2m^*$ and the Fermi momentum p_F is related to the mean particle density $\rho_0 = \rho_{0p} = \rho_{0n} = p_F^3/3\pi^2$. Integrating Eqs. (17) over the angles $\Omega_{\mathbf{p}}$ of the momentum $\mathbf{p}$ one has

$$\begin{aligned}\left[\tfrac{1}{2}F_{0,pp}(1-\Delta)w_p - 1\right]\Phi_p + \tfrac{1}{2}F_{0,pn}(1+\Delta)w_n\Phi_n = 0,\\ \tfrac{1}{2}F_{0,pn}(1-\Delta)w_p\Phi_p + \left[\tfrac{1}{2}F_{0,pp}(1+\Delta)w_n - 1\right]\Phi_n = 0,\end{aligned} \quad (20)$$

with

$$w_q = Q_1(s_q), \qquad Q_1(z) = \frac{z}{2}\ln\frac{z+1}{z-1} - 1. \quad (21)$$

Transforming Eqs. (17) and (18) into the isoscalar (+) and isovector (−) representation one can define

$$\nu_\pm = \nu_p \pm \nu_n, \quad \delta\rho_\pm = \delta\rho_p \pm \delta\rho_n, \quad \delta\mathbf{u}_\pm = \delta\mathbf{u}_p \pm \delta\mathbf{u}_n, \ldots. \quad (22)$$

Within this representation we introduce also the amplitudes

$$\Phi_\pm = \frac{2}{F_{0,pp}^2 - F_{0,pn}^2}[F_{0,pp}(\Phi_p \pm \Phi_n) - F_{0,pn}(\Phi_n \pm \Phi_p)]. \quad (23)$$

The set of homogeneous equations (20) leads to a dispersion relation [see Appendix C, Eq. (C3)]

$$\begin{aligned}&4F_0F_0'(F_0Q_1 - 1)(F_0'Q_1 - 1)\\ &\quad - \Delta^2F_0^2F_0'^2\Big/4\left(\frac{s^2}{s^2-1} + Q_1\right)^2 = 0,\end{aligned} \quad (24)$$

where one has used $s_p = s(1+\Delta)$ and $s_n = s(1-\Delta)$. The dispersion equation (24) provides two solutions for the sound velocity: $s = s^{(1)}$ and $s = s^{(2)}$. If we neglect the second-order terms in Δ in Eq. (24) we obtain the dispersion relations for two separated (isoscalar and isovector) modes

$$\begin{aligned}Q_1(s) &= 1/F_0 \quad \text{for } s = s^{(1)},\\ Q_1(s) &= 1/F_0' \quad \text{for } s = s^{(2)}.\end{aligned} \quad (25)$$

Note that the corrections to the solutions $s^{(1)}$ and $s^{(2)}$ of Eqs. (25) are linear in Δ. Moreover, as we will see in the following, the connection between the two sound modes can appear also as a result of the boundary conditions.

By using the τ approximation for the collision integral $\delta\mathrm{St}_\pm[f_p, f_n] \neq 0$ in both the isoscalar and isovector channels [see Eq. (A12), Appendix A] and assuming $F_1 \neq 0$, the dispersion relations of Eq. (25) can be easily generalized as (see also Refs. [22,24])

$$\begin{aligned}&\frac{i\omega\tau_+}{i\omega\tau_+ - 1}G_1 - Q_1(\zeta_+)\left[G_1\left(F_0 - \frac{1}{i\omega\tau_+ - 1}\right)\right.\\ &\quad\left. + \zeta_+^2\left(F_1 - \frac{3}{i\omega\tau_+ - 1}\right)\frac{i\omega\tau_+}{i\omega\tau_+ - 1}\right] = 0\\ &\quad \text{for} \quad s = s^{(1)},\\ &\frac{i\omega\tau_-}{i\omega\tau_- - 1} - Q_1(\zeta_-)\left[F_0' - \frac{1}{i\omega\tau_- - 1}\right.\\ &\quad\left. - \zeta_-^2\frac{3}{i\omega\tau_- - 1}\frac{i\omega\tau_-}{i\omega\tau_- - 1}\right] = 0 \quad \text{for} \quad s = s^{(2)}.\end{aligned} \quad (26)$$

Here $G_1 = m^*/m = 1 + F_1/3$, $\zeta_+(s) = s(1 + 1/\omega\tau_+)$, and $\zeta_-(s) = s(1 + 1/\omega\tau_-)$ and the relaxation times for the isoscalar and isovector modes (τ_+ and τ_-, respectively) are different.

The results of numerical solution of Eqs. (26) are presented in Fig. 1 as functions of $\omega\tau$. As seen from this figure, there is an essential difference between the solutions s for $F_0 = -0.2$ with $F_1 = 0.0$ (see broken line with open circles) and $F_1 = 0.6$ (solid line with open circle) and those with respect given by the solid curve with full circles for $s^{(2)}$ ($F_0' = 1.2$, $F_1' = 0$). The broken ($F_1 = 0.6$) line for s is similar to the $s^{(2)}$ solid curve because both the first-sound $\omega\tau \to 0$ and the zero-sound $\omega\tau \to \infty$ limits are real. This is not the case for the broken $F_1 = 0$ curve for which the zero-sound limit $\omega\tau \to \infty$ has a finite, nonzero, imaginary part usually associated with Landau damping at nonzero temperature [29].

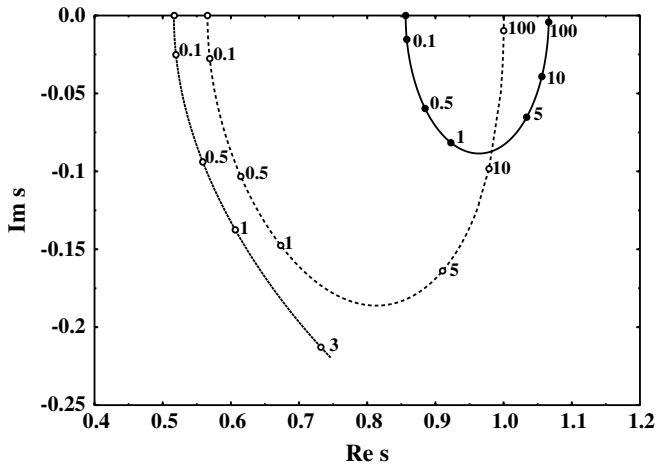

FIG. 1. Solutions of the dispersion equation (26) for $s^{(1)}$ and $s^{(2)}$ versus the $\omega\tau$ parameter (see numbers near the circles). The full points (solid line) are for the isovector-like sound velocity $s^{(2)}$ with the Landau parameters $F_0' = 1.2$, $F_{(1)}' = 0$. The open circles are for the isoscalar-like sound velocity $s^{(1)}$; solid line for $F_0 = -0.2$, $F_1 = 0.6$ and broken line for $F_0 = -0.2$, $F_1 = 0$.

C. Splitting into two sound waves

For both solutions $s = s^{(1)}$ and $s = s^{(2)}$ one can find the ratio of amplitudes of the isoscalar, Φ_+, and isovector, Φ_-, vibrations. Using Eqs. (C2)–(C5), one obtains

$$\left.\frac{\Phi_-^{(1)}}{\Phi_+^{(1)}}\right|_{s=s^{(1)}} = \frac{F_0[s^{(1)2}(1+F_0)-1]}{(F_0'-F_0)(s^{(1)2}-1)}\Delta,$$
$$\left.\frac{\Phi_+^{(2)}}{\Phi_-^{(2)}}\right|_{s=s^{(2)}} = \frac{F_0'[s^{(2)2}(1+F_0')-1]}{(F_0-F_0')(s^{(2)2}-1)}\Delta. \tag{27}$$

Finally, the amplitudes v_q in Eq. (17) are given by

$$v_q^{(\kappa)} = \frac{1}{4\pi}\frac{\cos\theta}{\cos\theta - s_q^{(k)}}\Phi_q^{(\kappa)}, \qquad (\kappa = 1, 2), \tag{28}$$

where

$$\Phi_q^{(1)} = \phi_1(1 \pm \Delta_1/2), \quad \Phi_q^{(2)} = \pm\phi_2(1 \pm \Delta_2/2), \tag{29}$$

$$\phi_1 = \frac{1}{2}F_0\Phi_+^{(1)}, \quad \Delta_1 = \frac{4F_0'[s^{(1)2}(1+F_0)-1]}{(F_0'-F_0)(s^{(1)2}-1)}\Delta, \tag{30}$$

$$\phi_2 = \frac{1}{2}F_0'\Phi_-^{(1)}, \quad \Delta_2 = \frac{4F_0[s^{(2)2}(1+F_0')-1]}{(F_0-F_0')(s^{(2)2}-1)}\Delta. \tag{31}$$

The amplitudes $\Phi_\pm^{(\kappa)}$ determine the isoscalar and isovector components of the relevant local quantities. For instance, for the isovector part of the particle density variation $\delta\rho_-^{(\kappa)}$ one obtains from Eqs. (11) and (22)

$$\delta\rho_-^{(1)} = \Delta\frac{2mi^L p_F}{\pi^2\hbar^3}\phi_1\frac{(F_0'+F_0)(s^{(1)2}-1)+F_0'(2F_0s^{(1)2}-1)}{(F_0'-F_0)(s^{(1)2}-1)} \times j_L(kr)Y_{L0}(\hat{r})e^{-i\omega t},$$
$$\delta\rho_-^{(2)} = \frac{2mi^L p_F}{\pi^2\hbar^3}\phi_2\, j_L(kr)Y_{L0}(\hat{r})e^{-i\omega t} \tag{32}$$

for $s = s^{(1)}$ and $s = s^{(2)}$, respectively. As seen from Eqs. (32), up to second-order terms in Δ the density amplitude of $\delta\rho_-^{(2)}$, related to the sound velocity $s = s^{(2)}$, is of zeroth order in Δ, whereas the amplitude of $\delta\rho_-^{(1)}$ for the $s = s^{(1)}$ solution is proportional to Δ and it disappears for the symmetric limit $N = Z$. For the isoscalar density $\delta\rho_+$ the density $\delta\rho_+^{(1)}$ from the sound wave velocity $s^{(1)}$ dominates whereas the $s^{(2)}$ density component $\delta\rho_+^{(2)}$ is of first order in Δ.

By using Eqs. (32) and similar expressions for the isoscalar mode, the ratios of the particle density variations $\delta\rho_\pm$ for both $s^{(1)}$ and $s^{(2)}$ solutions can be written as

$$\left.\frac{\delta\rho_-}{\delta\rho_+}\right|_{s=s^{(1)}} = \frac{2F_0'[s^{(1)2}(1+F_0)-1]}{(F_0'-F_0)(s^{(1)2}-1)}\Delta,$$
$$\left.\frac{\delta\rho_+}{\delta\rho_-}\right|_{s=s^{(2)}} = \frac{2F_0[s^{(2)2}(1+F_0')-1]}{(F_0-F_0')(s^{(2)2}-1)}\Delta \tag{33}$$

for $s = s^{(1)}$ and $s = s^{(2)}$, respectively. Note that in the symmetric limit $N \to Z$, $\Delta \to 0$ we have separation between isoscalar and isovector modes: According to Eqs. (33), the solution $s^{(1)}$ is related to the pure isoscalar motion ($\delta\rho_-^{(1)} \to 0$) and the $s^{(2)}$ velocity branch corresponds to the pure isovector vibrations, ($\delta\rho_+^{(2)} \to 0$) [see the second equation in Eq. (33)]. For asymmetric nuclear matter ($\Delta \neq 0$) both the isoscalar and isovector vibration amplitudes are not zero for the velocity $s^{(1)}$ but the isovector component is small compared to the isoscalar one [see Eqs. (33)]. The opposite situation takes place for the velocity $s^{(2)}$ for which, however, the relative contribution of the isoscalar mode to the isovector motion is much smaller, being proportional to the parameter Δ, according to Eqs. (33). We thus emphasize that for the asymmetrical case the isovector vibrations described by the density $\delta\rho_- \neq 0$ can be presented by both $s^{(1)}$ and $s^{(2)}$ sound waves (see Fig. 1) and the same for the isoscalar modes at $\delta\rho_+ \neq 0$. However, Eqs. (33) show that the isovector density variation $\delta\rho_-$ for the $s^{(1)}$ velocity branch is much smaller than that for the $s^{(2)}$ one for small Δ and otherwise for the isoscalar density $\delta\rho_+$.

D. Boundary conditions

For the finite Fermi liquid the dispersion relations (25) or (26) have to be complemented by the boundary conditions. In the following we will consider small vibrations of a nuclear surface about a spherical shape. The time-dependent nuclear radius $R(t)$ is given by

$$R(t) = R_0[1 + \alpha_s(t)Y_{L0}(\hat{\mathbf{r}})], \qquad \alpha_s(t) = \alpha_\omega e^{-i\omega t}, \tag{34}$$

where $R_0 = r_0A^{1/3}$ is the equilibrium radius of the nucleus and $Y_{L0}(\hat{r})$ are the spherical harmonics representing axially symmetric shapes. For small vibration amplitudes the boundary conditions on the free surface of the Fermi-liquid drop read [17]

$$u_{r,\pm}\Big|_{r=R_0} = R_0\dot{\alpha}_{s,\pm}Y_{L0}(\hat{\mathbf{r}}), \tag{35}$$
$$\delta\Pi_{rr,\pm}\Big|_{r=R_0} = \alpha_{s,\pm}\overline{\mathcal{P}}_{s,\pm}Y_{L0}(\hat{\mathbf{r}}) \tag{36}$$

(see Appendix E for their derivation). Here u_r and $\delta\Pi_{rr}$ are the radial components of the velocity field $\mathbf{u}$, Eq. (11), and momentum flux tensor $\delta\Pi_{\nu\mu}$, Eq. (16), respectively. The velocity field $\mathbf{u}_\pm$ and the momentum flux tensor $\delta\Pi_{\nu\mu,\pm}$ in the isoscalar-isovector representation are given by

$$\mathbf{u}_\pm = \mathbf{u}_p \pm \mathbf{u}_n, \qquad \delta\Pi_{\nu\mu,\pm} = \delta\Pi_{\nu\mu,\,p} \pm \delta\Pi_{\nu\mu,\,n}. \tag{37}$$

The surface pressures $\overline{\mathcal{P}}_{s,\pm}$ in Eq. (36) are given by

$$\overline{\mathcal{P}}_{s,+} = \frac{\rho_0 b_{s,+}}{3A^{1/3}}(L-1)(L+2),$$
$$\overline{\mathcal{P}}_{s,-} = \frac{2\rho_0 b_{s,-}A^{1/3}}{3}, \tag{38}$$
$$\rho_0 = \frac{p_F^3}{3\pi^2\hbar^3},$$

where $b_{s,+}$ and $b_{s,-}$ are constants. We point out that the self-consistency relation (E11), used in the derivation of the boundary condition (36), ensures that the total momentum (center of mass position) is conserved for both the isoscalar and the isovector modes (see also Ref. [30]).

Substituting Eqs. (D1)–(D3) into the boundary conditions (35) and (36) one obtains

$$-iv_F s_\kappa k R_0 \frac{\bar{\Pi}^{(\kappa)}_{rr,\pm}}{\bar{u}^{(\kappa)}_{r,+}} \alpha_{s,\pm} = \overline{\mathcal{P}}_{s,\pm} \alpha_{s,\pm}, \tag{39}$$

where $\bar{\Pi}^{(\kappa)}_{rr,\pm}$ and $\bar{u}^{(\kappa)}_{r,+}$ are given by Eqs. (D2) and (D3) and $\alpha_{s,\pm}$ are defined at the end of Appendix E. The solutions of Eq. (39) are split into the two parts:

$$\alpha_{s,+} = 0, \qquad \alpha_{s,-} \neq 0 \qquad \text{(IV)} \tag{40}$$

and

$$\alpha_{s,-} = 0, \qquad \alpha_{s,+} \neq 0 \qquad \text{(IS)}. \tag{41}$$

For the isovector modes (IV), for which we present numerical results, the secular equation (39) can be transformed to the following transparent form (see Appendix D):

$$\mathcal{D}^{(\kappa)}_L(\omega) = 0, \tag{42}$$

where

$$\mathcal{D}^{(\kappa)}_L(\omega) = j'_L(kR_0) - \tfrac{3}{2}\xi_- kR_0 \left[\mathcal{C}^{(\kappa)}_1 j''_L(kR_0) + \mathcal{C}^{(\kappa)}_2 j_L(kR_0)\right]. \tag{43}$$

In the case of isovector dipole excitations, $L = 1$, the lowest solutions to *both* equations (42) for $\kappa = 1$ ($s = s^{(1)}$) and 2 ($s = s^{(2)}$) give the energy of the main resonance peak, $\hbar\omega^{(2)}$, and its satellite, $\hbar\omega^{(1)}$. They can be found explicitly by expanding the spherical Bessel functions in power series to the third order, which provides a good approximation for the lowest resonances $kR \sim 1$,

$$\hbar\omega^{(1)} \approx \hbar\Omega \sqrt{\frac{10 s^{(1)2}}{3\left[1 + \xi_-\left(5\mathcal{C}^{(1)}_2 - 3\mathcal{C}^{(1)}_1\right)\right]}},$$
$$\hbar\omega^{(2)} \approx \hbar\Omega \sqrt{\frac{10\, s^{(2)2}}{3[1 + 2\xi_-(F'_0 + 2(s^{(2)})^2 + 1)]}}, \tag{44}$$

where

$$\Omega = \frac{v_F}{R_0} \approx \frac{\epsilon_F}{A^{1/3}\hbar} \tag{45}$$

and $\mathcal{C}^{(1)}_{1,2}$ are defined in Eqs. (D10). The energy $\hbar\omega^{(2)}$ of the main peak depends only on the isovector interaction constant F'_0 [also through $s^{(2)}$; see Eq. (25)] whereas the energy $\hbar\omega^{(1)}$ of the satellite depends on all isovector and isoscalar interaction constants. Note that there is a common reason for the presence of the isovector constant F'_0 in the resonance energies $\hbar\omega^{(1)}$ and $\hbar\omega^{(2)}$ of Eq. (44) because both of them belong to the isovector mode. The first (satellite) resonance energy $\hbar\omega^{(1)}$ in Eqs. (44) is also a function of the isoscalar interaction amplitudes F_0 and F_1 through the constants $\mathcal{C}^{(1)}_{1,2}$ of Eqs. (D10) and the sound velocity $s^{(1)}$, as a solution of the corresponding dispersion equation in Eqs. (26). We emphasize that the resonance energies $\hbar\omega^{(1)}$ and $\hbar\omega^{(2)}$ of Eqs. (44) are related to the *lowest* roots of different ($\kappa = 1$ and 2) secular equations (43), which have an infinite sequence of higher lying roots commonly known as overtones [31].

The energy splitting $\hbar\omega^{(1)} - \hbar\omega^{(2)}$ can be roughly estimated from Eqs. (44) for the case $s^{(1)} \approx s^{(2)} \approx 1$ for which both resonances are close to the zero sound regime. In this case the energies $\hbar\omega^{(\kappa)}$ of Eqs. (44) are simplified to

$$\hbar\omega^{(1)} \approx \hbar\Omega \sqrt{\frac{10}{3[1 + 2\xi_-(9 - 7F'_0)/3G_1]}},$$
$$\hbar\omega^{(2)} \approx \hbar\Omega \sqrt{\frac{10}{3[1 + 2\xi_-(3 + F'_0)]}}. \tag{46}$$

Both resonance energies $\hbar\omega^{(\kappa)}$ are mainly proportional to $A^{-1/3}$ through $\hbar\Omega$ but the quantity $\hbar\omega^{(1)}A^{1/3}$ increases slowly with A because of the additional $A^{-1/3}$ dependence of ξ_-, given after Eqs. (D8) [see Eqs. (46)]. We point out that such an A dependence of the IVGDR energies agrees with the experimental data (see Fig. 2 and more detailed discussion in Sec. IV). Using the power expansion in ξ_- in Eqs. (46), for large enough particle number A one obtains a simple estimate for the energy splitting,

$$\hbar\omega^{(1)} - \hbar\omega^{(2)} \approx \left(\frac{10}{3}\right)^{2/3} \frac{\epsilon_F^2}{b_{s,-}A^{2/3}G_1} \left[\left(1 + \frac{F_1}{10}\right) F'_0 + F_1\right]. \tag{47}$$

This result shows that the splitting effect depends significantly on the volume, F'_0, and surface, $b_{s,-}$, isovector interactions, and the effective mass through F_1, but does not depend on the neutron excess $N - Z$. However, as shown in the following, the ratio of the satellite strength to that of the main resonance for the isovector modes is largely proportional to the asymmetry parameter X. These results show essentially a new IVGDR splitting effect as compared to the one obtained in the traditional ISM and its modern extensions (see Refs. [19,20]), having a different energy splitting proportional to X^2.

III. RESPONSE FUNCTION AND STRENGTH SPLITTING

We also want to consider the excitations of nuclei in terms of the response to the external field

$$V_{\text{ext},q} = \mathcal{V}_{\text{ext},q}(\mathbf{r}, t) + [\mathcal{V}_{\text{ext},q}(\mathbf{r}, t)]^+, \tag{48}$$

by assuming

$$\mathcal{V}_{\text{ext},q}(\mathbf{r}, t) = \lambda^\omega_q(t) \frac{(2L+1)!!}{4\pi(ik)^L} \int d\Omega_{\mathbf{k}}\, e^{i\mathbf{k}\cdot\mathbf{r}} Y_{L0}(\hat{\mathbf{k}}),$$
$$\lambda^\omega_q(t) = \lambda^\omega_q \exp\left[-i(\omega + i\eta)t\right], \tag{49}$$

where $\eta \to +0$, λ^ω_q is the amplitude, and ω is the frequency of the external field. In the following we will consider the long-wavelength limit $kR_0 \ll 1$ with

$$\mathcal{V}_{\text{ext},q}(\mathbf{r}, t) = \lambda^\omega_q(t)\hat{Q}(\mathbf{r}), \quad \hat{Q}(\mathbf{r}) = r^L Y_{L0}(\hat{\mathbf{r}}) \quad \text{for} \quad L \geqslant 1. \tag{50}$$

The linear response function $\chi_q(\omega)$ can be determined through the Fourier transform $\langle\hat{Q}\rangle_\omega$ of the quantum average $\langle\hat{Q}\rangle_t$ by

$$\langle\hat{Q}\rangle_\omega = -\lambda^\omega_q \chi_q(\omega). \tag{51}$$

According to Eq. (51), one can express $\chi_q(\omega)$ in terms of the Fourier transform $\delta\rho_\omega(\mathbf{r})$ of the transition density $\delta\rho(\mathbf{r}, t)$ [22] as

$$\chi_q(\omega) = -\frac{1}{\lambda_q^\omega}\int d\mathbf{r}\,\hat{Q}(\mathbf{r})\,\delta\rho_q^\omega(\mathbf{r}). \tag{52}$$

Note that in macroscopic approaches the transition density $\delta\rho_q(\mathbf{r}, t)$ can be represented as a sum of a "volume" and a "surface" term (see Ref. [32]),

$$\delta\rho_q(\mathbf{r}, t) = \delta\rho_q^{\rm vol}(\mathbf{r}, t)y(R_0 - r) - \frac{\partial y(R_0 - r)}{\partial r}\rho_0\left[\delta R_q(\hat{\mathbf{r}}) - \frac{4\pi}{3}\,\delta\aleph\, Y_{10}(\hat{\mathbf{r}})\right], \tag{53}$$

where δR_q is the variation of nuclear radius with respect to the laboratory coordinate system $\mathbf{r} = (x, y, z)$ with the z axis, directed to the wave vector $\mathbf{k}$ [see Eq. (34)],

$$\delta R_q(\hat{\mathbf{r}}) = R_0\alpha_{s,q}Y_{L0}(\hat{\mathbf{r}}), \tag{54}$$

and

$$\delta\aleph = \frac{1}{A}\int d\mathbf{r}'\,r'\,Y_{10}(\hat{\mathbf{r}}')\left[\delta\rho_q^{\rm vol}(\mathbf{r}', t)\,y(R_0 - r') - \frac{\partial y(R_0 - r')}{\partial r'}\rho_0\,\delta R_q(\hat{\mathbf{r}}')\right]. \tag{55}$$

The upper index "vol" in $\delta\rho_q^{\rm vol}(r, t)$ in Eq. (53) indicates that this quantity is determined by the equations of motion in the nuclear volume that were considered in the previous section. The profile surface function $y(x)$ in Eq. (55) decreases from one to zero within the narrow region near $x = 0$ (see Refs [32–35]). The difference in square brackets of the second (surface) term in Eq. (53) is the radius displacement in the coordinate system of the center of mass. In this coordinate system, the spurious motion of the nuclear center of mass already excludes multipole vibrations of the Fermi-liquid drop because the radius displacement $\delta\mathbf{R}_{q,\rm c.m.}$ of the center of mass is identically zero in the laboratory coordinate system. Namely,

$$\delta\mathbf{R}_{q,\,\rm c.m.} = \frac{1}{A}\int d\,\mathbf{r}\,\mathbf{r}\,\delta\rho_q(\mathbf{r}, t) \equiv 0, \tag{56}$$

according to the definitions of Eqs. (53) and (55). The radius correction proportional to $\delta\aleph$ is zero for all multipolarities L, except for the dipole ($L = 1$) isoscalar modes for which it is important to remove a spurious $\omega = 0$ motion of the center of mass. The dynamical variations of the "volume" and "surface" parts of the transition density (53) cancel each other such that the c.m. position is conserved similarly as for the vibrations of a normal classical liquid drop. Note that there is no spurious motion at zero excitation energy for the isoscalar $L = 1$ mode because its strength in the FLDM is zero at $\omega \to 0$ for both the main peak and the satellite [see Eqs. (60) and (61)].

The solution $\delta f_q(\mathbf{r}, \mathbf{p}, t)$ of Eq. (3) is given by

$$\delta f_q(\mathbf{r}, \mathbf{p}, t) = \delta f_{{\rm hom},q}(\mathbf{r}, \mathbf{p}, t) + \delta f_{{\rm ext},q}(\mathbf{r}, \mathbf{p}, t), \tag{57}$$

where $\delta f_{{\rm ext},q}$ is the partial solution of the nonhomogeneous equations (3) and $\delta f_{{\rm hom},q}$ is the solution of the corresponding homogeneous equation. The quantity $\delta f_{{\rm hom},q}$ is given by Eq. (8). The partial solution $\delta f_{{\rm ext},q}$ can be taken in the form of superposition of plane waves similar to Eq. (8),

$$\delta f_{{\rm ext},q}(\mathbf{r}, \mathbf{p}, t) = \frac{(2L+1)!!}{4\pi(ik)^L}\lambda_q^\omega(t)\delta(\epsilon - \epsilon_{F,q}) \times \int d\Omega_{\mathbf{k}}\nu_{{\rm ext},q}(\hat{\mathbf{p}}\cdot\hat{\mathbf{k}})Y_{L0}(\hat{\mathbf{k}})e^{i\mathbf{k}\cdot\mathbf{r}}. \tag{58}$$

Substituting the solutions (57) and (58) into the derivations of the velocity field $\mathbf{u}$ and the momentum flux tensor $\delta\Pi_{\nu\mu}$ [Eq. (37)] and using the boundary conditions (35) and (36) one obtains the relations among the amplitudes $\Phi_\pm$, $\alpha_{s,\pm}$, and $\lambda_\mp^\omega = \lambda_p^\omega \pm \lambda_n^\omega$, similar to the previous derivation of Eq. (39). The difference is that we now obtain additional terms proportional to $\lambda_\mp$ on the left hand side of Eq. (39) that are related to the external field component $f_{{\rm ext},q}$ (58). The final result for the most interesting response isovector-like functions $\chi_-(\omega)$ in the long-wavelength limit $kR_0 \ll 1$ reads

$$\chi_{L,-}^{(\kappa)}(\omega) = \frac{\mathcal{A}_L^{(\kappa)}(k)}{\mathcal{D}_L^{(\kappa)}(\omega)}, \qquad k = \omega/v_F s^{(\kappa)}. \tag{59}$$

The solutions to the characteristic equation (42) [with Eq. (43)] provide the complex poles of the response function $\chi_{L,-}^{(\kappa)}(\omega)$ at $\omega_{\rm res} = {\rm Re}(\omega_{\rm res}) + i{\rm Im}(\omega_{\rm res})$. The damping of the collective vibrations at ${\rm Im}(\omega_{\rm res}) \neq 0$ is due to the collision integral in Eq. (3). For both solutions $s = s^{(1)}$ and $s = s^{(2)}$ the amplitudes $\mathcal{A}_L^{(\kappa)}(k)$ are given by

$$\mathcal{A}_L^{(1)}(k) = -\frac{6\rho_0 R_0^{L+4}\xi_-\Delta}{5\epsilon_F kR_0\mathcal{C}}[\mathcal{C}_3 j_L(kR_0) - kR_0\,(\mathcal{C}_3 + \mathcal{C})\,j_L'(kR_0)], \qquad \mathcal{C}_3 = (F_0 - F_0' - Q_1)\mathcal{K} - Q_1^2, \tag{60}$$

$$\mathcal{A}_L^{(2)}(k) = -L^2\left[1 + \frac{12\xi_-(L-1)}{5(L+2)}\right]\frac{\rho_0 R_0^{2L+1}}{m\omega^2} \times j_L(kR_0)\,[1 + \mathcal{O}(\Delta)], \quad \omega = v_F s^{(2)}k, \tag{61}$$

where $\mathcal{K} = s^{(1)2} - 1$.

For widths $\Gamma = -2\hbar{\rm Im}(\omega_{\rm res})$ that are small compared to those of the resonance energies $\hbar{\rm Re}(\omega_{\rm res})$ one can use the expansion in $\Gamma/\hbar{\rm Re}(\omega_{\rm res})$ near the poles $\omega_{\rm res} = \omega_{{\rm res},i}$ and obtain the isovector-like strength function $\mathcal{S}_-^{(\kappa)}$ as

$$\mathcal{S}_{L,-}^{(\kappa)}(\omega) = -\frac{1}{\pi}{\rm Im}\chi_{L,-}^{(\kappa)}(\omega) = \sum_i \frac{\mathcal{A}_L^{(\kappa)}\left(k_{L,i}^{(\kappa)}R_0\right)}{\pi\left|\mathcal{D}_L^{(\kappa)\prime}\right|_{\omega=\omega_{L,i}^{(\kappa)}}|} \times \frac{\Gamma_{L,i}^{(\kappa)}/2\hbar}{\left(\mathcal{D}_L^{(\kappa)}(\omega)/\mathcal{D}_L^{(\kappa)\prime}\big|_{\omega=\omega_{L,i}^{(\kappa)}}\right)^2 + \left(\Gamma_{L,i}^{(\kappa)}\right)^2/4\hbar^2}, \tag{62}$$

where $\omega_{L,i}^{(\kappa)} = {\rm Re}(\omega_{L,i}^{(\kappa)}) - i\Gamma_{L,i}^{(\kappa)}/2\hbar$ are the complex solutions of the secular equation (42) related to the $s = s^{(\kappa)}$. The derivatives of the $\mathcal{D}_L^{(\kappa)}$ in Eq. (62) are taken over dimensionless kR_0.

Integrating Eq. (62) over ω with the weight function one obtains the energy n-moments of the strength function

$$m_{L,n}^{(\kappa)} = \hbar^{n+1} \int d\omega \omega^n \mathcal{S}_{L,-}^{(\kappa)}(\omega) \approx \left(\frac{\hbar v_F s^{(\kappa)}}{R_0}\right)^{n+1} \frac{\left(k_L^{(\kappa)} R_0\right)^n \mathcal{A}_L^{(\kappa)}\left(k_L^{(\kappa)} R_0\right)}{\left|\mathcal{D}_L^{(\kappa)\prime}\right|_{\omega=\omega_{L,i}^{(\kappa)}}|}. \quad (63)$$

Here we have restricted the sum over eigenfrequencies in Eq. (62) to the main lowest solutions $k_L^{(\kappa)}$ of the secular equation (42). For the isovector dipole and the lowest energy solution, $i = 1$, one obtains from Eqs. (63) for $n = 1$ (omitting indexes $L = 1$ and $i = 1$ in the eigenfrequencies)

$$\frac{m_1^{(2)}}{m_{\rm GDR}} = \frac{2 j_L(k^{(2)} R_0) A}{(k^{(2)} R_0)^2 \, |\mathcal{D}^{(2)\prime}|_{\omega=\omega^{(2)}}| N}, \quad m_{\rm GDR} = \frac{3}{4\pi} \frac{\hbar^2}{2m} \frac{N}{A} A, \quad (64)$$

$$\frac{m_1^{(1)}}{m_{\rm GDR}} = -\frac{12A}{5N} \frac{\epsilon_F s^{(1)2}}{(2 + \Delta_1/\Delta) b_{s,-} A^{1/3}} \times \frac{(1 - \Delta_1/\Delta) j_L(k^{(1)} R_0) - 3k^{(1)} R_0 \, j_L'(k^{(1)} R_0)}{|\mathcal{D}^{(2)\prime}|_{\omega=\omega^{(1)}}|} \Delta, \quad (65)$$

where $m_{\rm GDR}$ is the model-independent isovector energy-weighted sum rule (EWSR). (See Eq. (6.176) of Ref. [17]). Our transition density is normalized by the nuclear mass A instead of the charge eZ in Eq. (6.176) of Ref. [17]; the weight factor 3 and electron charge e are omitted in line of the definition of our multipole operator Eq. (49); the N/A factor written explicitly excludes any c.m. motion.) Note that if nonlocal forces depend on the velocity [terms $F_{\ell \neq 0, qq'}$ for the Landau's forces of Eqs. (6) and (7)] the isovector EWSR $m_{\rm GDR}$ in Eq. (64) is multiplied by an enhancement factor (see Eq. (3.39) of Ref. [36]). The enhancement factor is force dependent; that is, it is model dependent. To simplify our presentation, it is more convenient for us to use in Eq. (64) the model-independent value of $m_{\rm GDR}$ from Ref. [17]. We point out however that our calculations of the energy-weighted sums $m_1^{(1)}$ and $m_1^{(2)}$ in Eqs. (64) and (65) take into account the contributions from $m^* \neq m$ owing to the velocity-dependent forces [for instance, terms with F_1 in Eqs. (26) and (47)].

The main dipole resonance ($\kappa = 2, L = 1$) of the zero order in Δ [see Eqs. (63) and (61)] exhausts most of the EWSR: $m_1^{(2)}/m_{\rm GDR} \approx 1$. The strength of the other (satellite) resonance ($\kappa = 1$) is linear in Δ and is relatively small compared to the main peak. Within the same approximation, applied in the derivation of splitting Eq. (47), one has a simple estimation of their strength ratio as $m_1^{(1)}/m_{\rm GDR} \approx 32\epsilon_F(1 + F_0')X/3b_{s,-}A^{1/3}$. Note that the relative strength of such a satellite increases with the asymmetry parameter X and decreases with an increase of A. It depends also on the surface ($b_{s,-}$) and volume (F_0') isovector constants. As already noted, from Eq. (65) we realize that the strength of the satellite peak tends to zero, and in this sense, it disappears in the symmetric limit $N = Z$.

IV. NUMERICAL CALCULATIONS AND DISCUSSION

We will present results of some numerical calculations based on the analytical results of the previous sections. Figure 2 shows the IVGDR energy, $E_{\rm GDR} = \hbar\omega^{(2)}$, and the corresponding fraction of the EWSR, $m_{\rm GDR}$, [17] versus the mass number A for certain isotopes near the β-stability line [37–39]. Besides the well-known deformation splitting of the IVGDR energies in the rare earth ($A \approx 140-190$) and actinide ($A \approx 220$–240) elements discussed earlier in Refs. [6,7,12,15], the remaining full points represent the IVGDR characteristics of the main peaks obtained by different experimental groups cited in Refs. [37–39]. These points for spherical-like nuclei are in a good agreement with our FLDM results for the main

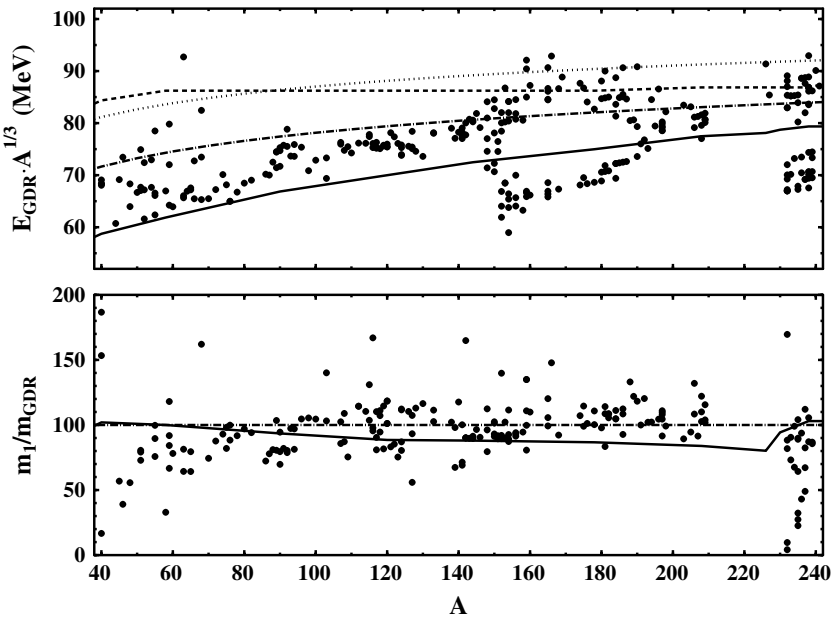

FIG. 2. Giant dipole resonance energies $E_{\rm GDR}$ multiplied by $A^{1/3}$ (top) and exhaustion $m_1^{(\kappa)}/m_{\rm GDR}$ of the EWSR $m_{\rm GDR}$ of Eq. (64) (in percent, bottom) for the main isotopes along the β-stability line vs the particle number A. The full points are the experimental data from Refs. [37–39] (see http://depni.npi.msu.su/cdfe/). The solid and broken lines are the main GDR resonances and their satellites obtained from Eq. (42) with Eq. (43) for $F_0' = 0.6$, $F_0 = -0.46$, $F_1 = -0.9$, $b_{s,-} = 78$ MeV, $r_0 = R_0/A^{1/3} = 1.1$ fm, and $\tau = 1.05 \times 10^{-22}$ s. Points and lines correspond to the estimations (44).

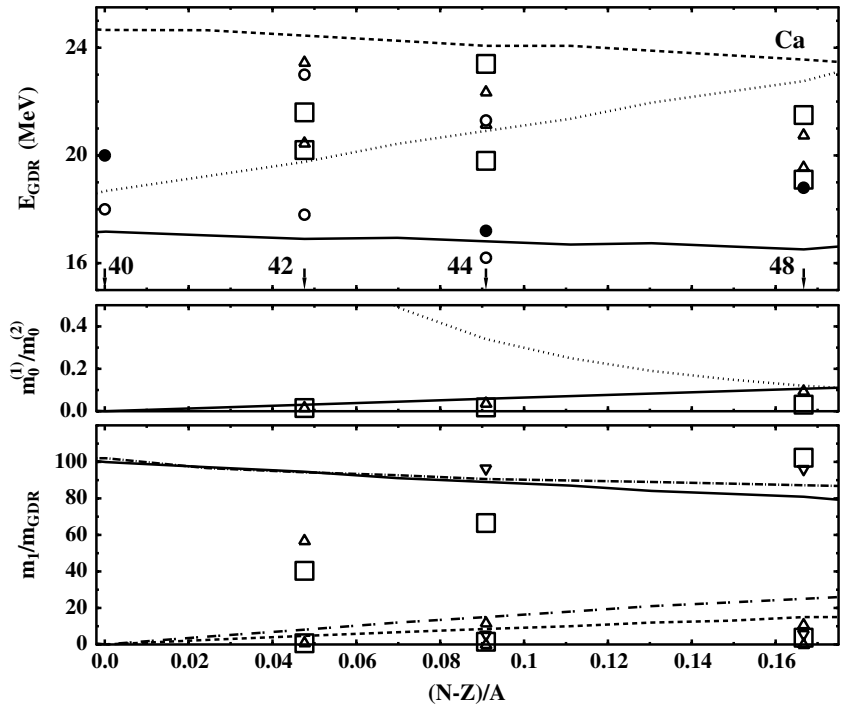

FIG. 3. Isovector giant dipole resonance energies $E_{\rm GDR}$ (top), EWSR exhaustion $m_1^{(\kappa)}/m_{\rm GDR}$ (bottom, in percent), and satellite strength $m_0^{(1)}$ divided by the main peak $m_0^{(2)}$ (middle) for the Ca isotopes vs the asymmetry parameter $X = (N - Z)/A$. The full and open circles show the experimental data from Refs. [37–39] and Ref. [7], respectively. The squares, triangles, and inverted triangles are obtained from the cross sections for the corresponding (γ, n) and (γ, p) reactions of Refs. [3,5,6,11], as explained in the text. The dots in the top and middle panels present the ISM. The solid and broken lines lines in the bottom panel show the analytical (exact integral) EWSR exhaustion (63) for the main IVGDR and satellites. The broken-dotted line and frequent broken-dotted line denote the approximations (64) and (65). Other notations and parameters are the same as in Fig. 2.

IVGDR energies $E_{\rm GDR}$ and the corresponding fraction of the EWSR along the β-stability line [see Eqs. (42) and (64)]. They were obtained by solving the secular equation Eq. (42) for $\kappa = 2$ with the sound velocity $s^{(2)}$ from Eqs. (26) for the particular choice of the isovector interaction parameters $F_0' = 0.6$, which corresponds to the symmetry energy constant $b_{\rm sym} \approx 30$ MeV. In this work we have adopted the values of $r_0 = 1.1$ fm and $b_{s,-} = 78$ MeV. The effective nucleon mass m_q^* was taken as $m_q^* = 0.7m$, which corresponds to the Landau parameter $F_1 = -0.9$. For the isoscalar interaction parameter F_0, which strongly influences the calculated satellite energy and the isovector dipole resonance splitting, we have used $F_0 = -0.5$ to have a reasonable value of the incompressibility coefficient $K = 6\epsilon_F(1 + F_0)$ of the nuclear matter of the order of 200 MeV. For simplicity, our numerical calculations were performed by assuming the simplest τ approximation for the collision integral with $\tau_{pp} = \tau_{nn} = \tau_{pn} = \tau \approx 1.1 \times 10^{-22}$ s (see also Appendix A). The relaxation time τ enters the secular equation (42) through the roots of the dispersion equations (26). The finite relaxation time τ provides the collisional width $\Gamma^{(\kappa)}$ of the IVGDR strength function $\mathcal{S}^{(\kappa)}(\omega)$ in Eq. (62).

The additional contributions into the IVGDR characteristics appear as a result of the coupling of the equations of motion (3) at $\Delta \neq 0$. The quantity $E_{\rm GDR}A^{1/3}$ of the main resonances approach the A-independent constant of the Steinwedel-Jensen (SJ) model for large particle numbers A at the value of $\approx$80 MeV and becomes a slightly decreasing function of A for light nuclei, similarly to those of the Goldhaber-Teller (GT) model. At the top of Fig. 2 we plot also the energy $\hbar\omega^{(1)}$ of the satellite evaluated using the secular equation (42) for $\kappa = 1$. As seen from Fig. 2, the satellites (broken line) appear at higher energies close to the main peaks (solid line) and the magnitude of the splitting is almost independent of the asymmetry parameter X, in the first order of Δ. The satellite energies multiplied by $A^{1/3}$ almost do not depend on the particle number A and the magnitude of splitting decreases slowly with increasing A. Note that a very strong splitting effect is seen from Fig. 2 in the rare-earth nuclei with $A \sim 150$–180, which is well explained in Ref. [16] as another remarkable phenomenon related to their deformations. A simple estimate for the energies $\hbar\omega^{(2)}$ and $\hbar\omega^{(1)}$ of Eqs. (45) shown in Fig. 2 for $\tau \to \infty$ (see Fig. 1) is in rather good agreement with the exact solutions of the secular equations (42). The value of the energy-weighted sum $m_1^{(2)}$ [Eq. (63)] for the main ($s = s^{(2)}$) IVGDR (see the bottom of Fig. 2) depletes more than 50% of the dipole sum rule $m_{\rm GDR}$ of Eq. (64). Thus, our FLDM predicts that the main IVGDR is related to Fermi-liquid vibrations with sound velocity $s^{(2)}$.

The values of $\omega\tau$ at the position of the main resonance is approximately 1.4–1.7 in our calculations with the collision relaxation time τ mentioned previously. This is an intermediate region between the hydrodynamic ($\omega\tau \ll 1$) and zero sound ($\omega\tau \gg 1$) collision regimes. We point out that the afore mentioned similarity of the FLDM results for the IVGDR to the ones obtained for the SJ and GT hydrodynamic-like models [16] can be explained by the closeness of the IVGDR modes to the hydrodynamic regime rather than to the zero sound one.

The main, $\hbar\omega^{(2)}$, and satellite, $\hbar\omega^{(1)}$, IVGDR energies, their relative strength $m_0^{(1)}/m_0^{(2)}$ (where $m_0 = \int_0^\infty dE\mathcal{S}_-(E)$ measures the $E1$ transition probability), and the depletion of the EWSR versus the asymmetry parameter X are presented in Figs. 3, 4, and 5 for several Ca, Sn, and Sm isotopes. They are compared with our interpretation of the experimental data in terms of the two-peak structure of the (γ, n) integral cross sections [the same for the (γ, p) reactions]. The joined points indicating the mean IVGDR energies are taken from

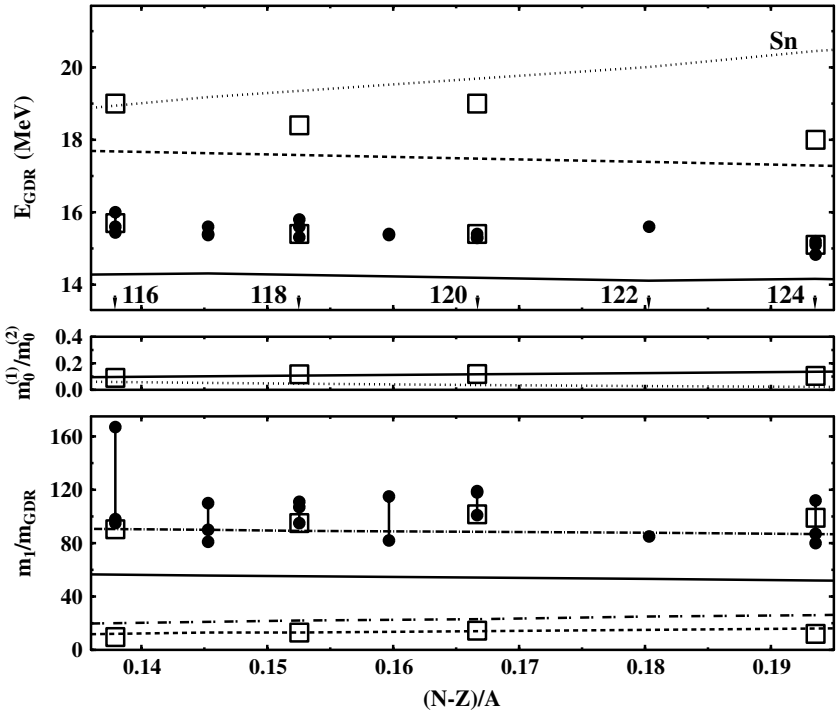

FIG. 4. The same as Fig. 3 for the Sn isotopes. The full joined circles show the experimental data from Refs. [37–39] of different groups (see the references therein). The squares and triangles are obtained from the integral cross sections of Ref. [2] and Ref. [12], respectively.

Refs. [37–39]. We emphasize that we are talking about the two-peak structure of the IVGDR for each reaction (γ, n) and (γ, p) independently rather than about comparison of the main peaks from both isospin conjugate reactions (γ, n) and (γ, p) as was done in the case of the ISM (see Ref. [7]). Moreover, we do not show in Figs. 3, 4, and 5 the corresponding experimental data for the ISM analysis of the splitting in (γ, n) and (γ, p) reactions and keep only the relevant data for the splitting phenomena in the FLDM. For instance, the squares in Figs. 3 and 4 were found, respectively, from the energy dependence of the cross section of the photo-neutron (γ, xn) reactions for Ca isotopes, in Refs. [3,5,6,11], and for Sn ones, in Refs. [2,12] [triangles in Fig. 3 were found from the (γ, xp) reactions]. All squares, triangles, and open circles have been obtained by the two Lorentzian fits of the corresponding cross sections. The energy interval for the mean-square fit includes the main peak and the wide bump on its right-hand side, which is interpreted as the satellite. For the case of the neutron cross sections with the deformed targets ^{42,44}Ca [3,6,11], the fitting procedure is applied for the second broader maximum,

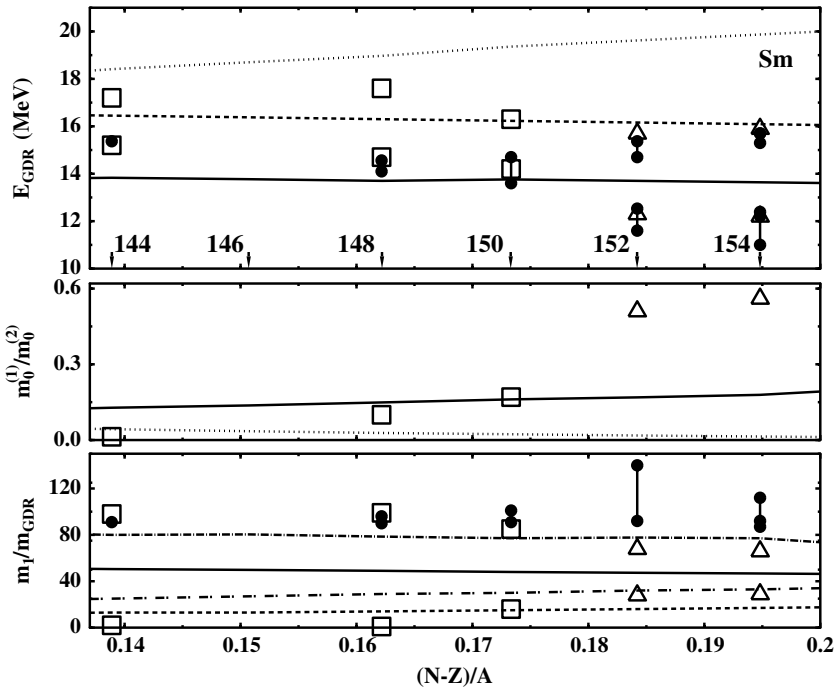

FIG. 5. The same as Fig. 3 for the Sm isotopes. The squares and triangles are obtained from the integral cross sections of Refs. [37–39] and Ref. [15], respectively.

which is interpreted as a sum of the main peak and its satellite strength. The squares in Fig. 5 for the Sm isotopes are similar to the ones obtained in Figs. 3 and 4 but the triangles show a double-resonance structure of another nature, which is due to nuclear deformation. We emphasize the difference between our FLDM splitting for the spherical-like nuclei ^{144}Sm, ^{148}Sm, and ^{150}Sm and the deformation splitting of the strongly deformed ^{152}Sm and ^{154}Sm isotopes.

As seen from the top of Figs. 3, 4, and 5, the magnitude of the IVGDR splitting in our FLDM does not depend on the neutron excess $N - Z$ and there is good agreement with our presentation of the experimental data (squares and triangles). Its slow decrease with the asymmetry parameter X is explained by the A dependence in Eqs. (47). This is in contrast to another splitting effect predicted by the ISM, which shows an increase of the energy splitting of the IVGDR with the isospin quantum number $T_3 = (N - Z)/2$ (see Refs. [3–11]).

The satellite strength ratio $m_0^{(1)}/m_0^{(2)}$ in the middle of Figs. 3, 4, and 5 is small and increases linearly with the asymmetry parameter X. This is quite different from both the case of the opposite ISM-splitting behavior $m_0^{(1)}/m_0^{(2)} \approx 1/T_3$ discussed for instance in [7] and the case of splitting caused by deformation with approximately equal peak strengths ($m_0^{(1)}/m_0^{(2)} \approx 1$) [16]. The bottoms of Figs. 3, 4, and 5 show the depletions of the EWSR; these are about constant for the main IVGDR and are proportional to the asymmetry parameter X for much smaller satellite contributions. The relative strengths and the depletion of the EWSR for all (Fermi-liquid) satellites decrease to zero and disappear in the symmetric limit $X \to 0$. As shown in Figs. 3, 4, and 5, the strength ratios $m_0^{(1)}/m_0^{(2)}$ of the two peaks and their depletions of the EWSR are in good agreement with the experimental results represented by the squares or the triangles. The strength maximum of the satellite is much smaller than the one of the main peak. However, the contributions of the satellite to the zeroth, $m_0^{(1)}$, and first, $m_1^{(1)}$, moments of the strength function are quite significant because of its much larger width. The small values of both the main and satellite EWSR depletions for the (γ, p) reactions with ^{44}Ca and ^{48}Ca targets (the triangles in the bottom of Fig. 3) are explained by the small total strength (EWSR depletion of about 0.1) compared to the estimate of $m_{\rm GDR}$ in Eq. (64). Note that this is not a typical situation for the IVGDR, which usually depletes the main part of the EWSR. The inverted triangles in the bottom of Fig. 3 show the result of our fitting procedure for ^{44}Ca and ^{48}Ca targets in (γ, p) reactions [3,6,11] using the normalization to 100% EWSR contribution from the IVGDR and its satellite. Finally, the open circles in Fig. 3, which we found from the inelastic (e, e') reactions with the ^{42}Ca and ^{44}Ca targets (see [7]) can be also explained by the FLDM splitting of the IVGDR. At least the magnitude of splitting and its weak dependence on the asymmetry parameter X are well described within the FLDM .

Note that the FLDM isovector splitting increases with the relaxation time τ such that the energy of the main peak decreases while the energy of the satellite increases. For the commonly accepted value of $b_{\rm sym}$ (fixed by the parameter F_0') the position of the main peak is determined mainly by the isovector surface parameter b_{S-}. The isoscalar interaction parameter F_0, related to the incompressibility coefficient of the nuclear matter, significantly affects only the position of the satellite. The strengths of both peaks depend on all these parameters. We emphasize that it is important to take into account the effective mass $m^* \neq m$ (nonzeroth parameter F_1), which influences the characteristics of both peaks owing to the dispersion and secular relations. In particular, the effective mass enhances the spreading of the main and satellite peaks.

V. CONCLUSIONS

The FLDM predicts the existence of two kinds of isovector (or isoscalar) vibrations related to the two different velocities $s^{(1)}$ and $s^{(2)}$ in a nuclear Fermi liquid. The sound velocities are determined by the isoscalar, F_0, and the isovector, F_0', Landau interaction amplitudes. The FLDM shows a satellite structure of the isovector and isoscalar resonances. We pointed out that the FLDM energy splitting of the isovector IVGDR does not depend on the neutron excess at the linear order in X. Moreover, the satellite structure of the isovector IVGDR does not depend on the type of reaction [(γ, xn), (γ, xp), or inelastic electron scattering] and can be found in each type of reaction and for spherical targets, in addition to the ISM and the dynamic collective model predictions. The isovector splitting appears essentially as a result of the asymmetry effect in the collective FLDM dynamics and is determined by the isovector volume, F_0', and surface, $b_{s,-}$, interactions, and the effective mass $m^* \neq m$ at $F_1 \neq 0$. The lowest peak depletes almost 100% of the EWSR and the other peak (the satellite) is associated with a significantly smaller contribution to the EWSR, which is proportional to the asymmetry parameter X.

ACKNOWLEDGMENTS

We thank S. V. Lukyanov, H. Toki, and V. A. Zheltonozhsky for useful and fruitful discussions. One of us (V.M.K.) acknowledges the nice hospitality of the Cyclotron Institute at Texas A&M University. This work was supported in part by the U.S. Department of Energy under Grant No. DOE-FG03-93ER40773, the U.S. National Science Foundation under Grant No. 0355200, and the Deutsche Forschungsgemeinschaft under Contract No. 436 UKR 113/66/0-1.

APPENDIX A: COLLISION INTEGRAL FOR A TWO-COMPONENT SYSTEM

For the calculation of the collision integral $\delta{\rm St}_q[f_p, f_n]$ we will follow Ref. [40]. We employ a relaxation time approximation (τ approximation) by assuming that the distribution function f_q in $\delta{\rm St}_q[f_p, f_n]$ relaxes to the *local* equilibrium distribution function

$$f_q^{\rm loc.eq} = \frac{1}{\exp\left[\left(\epsilon_q^{\rm loc.eq} - \mu_q^{\rm loc.eq} - \mathbf{p}\cdot\mathbf{u}_q\right)/T\right]}. \qquad \text{(A1)}$$

Here $\epsilon_q^{\rm loc.eq} = p^2/2m^* + \delta V_q$ is the single particle energy that is consistent with the distribution function $f_q^{\rm loc.eq}$ in regard to the variation δV_q of the self-consistent mean field. The chemical potential $\mu^{\rm loc.eq}$ is also consistent with the local equilibrium

distribution $f_q^{\rm loc.eq}$ providing $\int 2d\mathbf{r}\,d\mathbf{p} f_q^{\rm loc.eq}(\mathbf{r},\mathbf{p})/(2\pi\hbar)^3 = A_q$, with $A_p = Z$ and $A_n = N$. The function $f_q^{\rm loc.eq}$ of Eq. (A1) is a simple case of the general form $f(r,[p - mu]^2)$ for the equilibrium distribution function as applied to the system with linearization in the velocity field u (see Refs. [40,41]). The linearized collision integral $\delta{\rm St}_q[f_p, f_n]$ takes then the following form (see also Ref. [40]):

$$\delta{\rm St}_q[f_p, f_n] = -\sum_{q'} \frac{\delta f_{q'}^{\rm loc}}{\tau_{qq'}}, \quad \delta f_q^{\rm loc} = f_q - f_q^{\rm loc.eq}, \quad \text{(A2)}$$

where $\tau_{qq'}$ is the relaxation time caused by the interaction of particles in the qq' channel (pp, nn, pn, or np). As noted in the main text, we assume $\tau_{pp} = \tau_{nn}$ and $\tau_{pn} = \tau_{np}$. In the specific calculations, the collision integral of Eq. (A2) ensures the conservation of the particle number, the total momentum, and the total energy [40] for a two-component system.

We point out that, in contrast to Eq. (A2), the variation $\delta f_q = f_q - f_{{\rm eq},q}$ of the distribution function in the left-hand side of Eq. (3) is determined with respect to the *global* function $f_{{\rm eq},q}$ given by

$$f_{{\rm eq},q} = \frac{1}{\exp[(\epsilon_q - \mu_q)/T]}. \quad \text{(A3)}$$

The variations $\delta f_q^{\rm loc}$ and δf_q are related to each other by

$$\delta f_q = \delta f_q^{\rm loc} + \delta f_q^{\rm loc.eq}, \quad \text{(A4)}$$

where

$$\delta f_q^{\rm loc.eq} = f_q^{\rm loc.eq} - f_{{\rm eq},q} \approx \frac{\partial f_{{\rm eq},q}}{\partial \epsilon_q}(-\mathbf{p}\cdot\mathbf{u}_q - \delta\mu_q + \delta V_q),$$
$$\delta\mu_q = \mu_q^{\rm loc.eq} - \mu_q. \quad \text{(A5)}$$

We will also use an expansion of the dynamic distribution function $\delta f_q(\mathbf{r},\mathbf{p},t)$ in the spherical harmonic series in momentum space [21,22],

$$\delta f_q(\mathbf{r},\mathbf{p},t) = \sum_{l=0}^{\infty} \alpha_{l,q} Y_{l0}(\hat{\mathbf{p}}\cdot\hat{\mathbf{k}}) \frac{\partial f_{{\rm eq},q}}{\partial\epsilon_q} e^{-i(\omega t - \mathbf{k}\cdot\mathbf{r})}$$
$$\equiv \sum_{l=0}^{\infty} \delta f_{l,q}(\mathbf{r},\mathbf{p},t), \quad \text{(A6)}$$

where l is the multipolarity of the Fermi-surface distortion and

$$\delta f_{l,q}(\mathbf{r},\mathbf{p},t) = \alpha_{l,q} Y_{l0}(\hat{\mathbf{p}}\cdot\hat{\mathbf{k}}) \frac{\partial f_{{\rm eq},q}}{\partial\epsilon_q} e^{-i(\omega t - \mathbf{k}\cdot\mathbf{r})}. \quad \text{(A7)}$$

Using Eqs. (11), the expansion (A6), and the continuity equation

$$\frac{\partial}{\partial t}\rho_q + \nabla\cdot\rho_q\mathbf{u}_q = 0, \quad \text{(A8)}$$

one can obtain

$$\mathbf{p}\cdot\mathbf{u}_q = -\alpha_{1,q} Y_{10}(\hat{\mathbf{p}}\cdot\hat{\mathbf{k}}) e^{-i(\omega t - \mathbf{k}\cdot\mathbf{r})},$$
$$\delta\mu_q - \delta V_q = -\alpha_{0,q} Y_{00}(\hat{\mathbf{p}}\cdot\hat{\mathbf{k}}) e^{-i(\omega t - \mathbf{k}\cdot\mathbf{r})}. \quad \text{(A9)}$$

Using Eqs. (A5), (A7), and (A9), we obtain

$$\delta f_q^{\rm loc.eq} = \sum_{l=0}^{1} \delta f_{l,q}(\mathbf{r},\mathbf{p},t). \quad \text{(A10)}$$

Finally, by substituting Eqs. (A4), (A6), and (A10) into Eq. (A2) the collision integral takes the following form:

$$\delta{\rm St}_q[f_p, f_n] = -\sum_{q'}\sum_{l=2}^{\infty} \frac{\delta f_{l,q'}}{\tau_{qq'}}. \quad \text{(A11)}$$

By using Eq. (A11), the collision integral for the isoscalar channel, $\delta{\rm St}_+[f_p, f_n]$, and the isovector one, $\delta{\rm St}_-[f_p, f_n]$, can be written as

$$\delta{\rm St}_+[f_p, f_n] = -\sum_{l=2}^{\infty} \frac{\delta f_{l,+}}{\tau_+}, \quad \delta{\rm St}_-[f_p, f_n] = -\sum_{l=2}^{\infty} \frac{\delta f_{l,-}}{\tau_-}, \quad \text{(A12)}$$

where

$$\frac{1}{\tau_+} = \frac{1}{\tau_{pp}} + \frac{1}{\tau_{pn}}, \qquad \frac{1}{\tau_-} = \frac{1}{\tau_{pp}} - \frac{1}{\tau_{pn}}. \quad \text{(A13)}$$

We point out that the collision integral $\delta{\rm St}_q[f_p, f_n]$ of Eq. (A11) for a two-component system does not contain contributions from the monopole ($l = 0$) and dipole ($l = 1$) distortion of the Fermi surface providing conservation of the particle number and the total momentum. This result is similar to the one for the one-component system [21,24,40,41]. It is due to the general definition [41] that the collision integral disappears at the local (not global) equilibrium distribution. Namely [see also Eq. (A2)],

$${\rm St}_q\left[f_p^{\rm loc.eq}, f_n^{\rm loc.eq}\right] = 0. \quad \text{(A14)}$$

Note also that the presence of the $l = 1$ component itself in the collision integral for the isovector (dipole) vibrations does not contradict momentum conservation if the collision integral disappears at the global equilibrium (A3) instead of the condition (A14).

APPENDIX B: THE DERIVATION OF THE FERMI ENERGY SPLITTING

1. The β-stability condition

We begin from the Weizsäcker's formula by writing only the important terms:

$$E = E_{\rm vol}(A) + E_{\rm surf}(A) - b_{\rm sym}\frac{(N-Z)^2}{A} + E_{\rm Coul}(A,Z) + \ldots. \quad \text{(B1)}$$

We use here the symmetry energy coefficient $b_{\rm sym} = 30$ MeV. For the proton and the neutron separation energies S_q one has from (B1)

$$S_n = \frac{\partial E}{\partial N} = S_{\rm vol} + S_{\rm surf} - 2b_{\rm sym}X,$$
$$S_p = \frac{\partial E}{\partial Z} = S_{\rm vol} + S_{\rm surf} + 2b_{\rm sym}X + \bar{V}_{\rm Coul}, \quad \text{(B2)}$$

where

$$\bar{V}_{\rm Coul} = \frac{\partial E_{\rm Coul}}{\partial Z}. \tag{B3}$$

The β-stability condition reads

$$S_n = S_p. \tag{B4}$$

From Eqs. (B2), (B3), and (B4), one obtains

$$\bar{V}_{\rm Coul} = -4b_{\rm sym}X. \tag{B5}$$

2. Fermi energy splitting

The Fermi energy splitting $\Delta = (\epsilon_{F,n} - \epsilon_{F,p})/2\epsilon_F = \Delta_{\rm kin} + \Delta_{\rm pot}$ is a sum of the kinetic and potential parts. The kinetic part $\Delta_{\rm kin}$ is given by

$$2\Delta_{\rm kin} = (\epsilon_{F0,n} - \epsilon_{F0,p})/\epsilon_F = \left[p_{F,n}^2 - p_{F,p}^2\right]/2m^*\epsilon_F, \tag{B6}$$

where we have assumed $m_n^* \approx m_p^* \approx m^*$. The potential part $\Delta_{\rm pot}$ is due to the isotopic shift in the mean field,

$$\begin{aligned} 2\Delta_{\rm pot} = (V_n - V_p)/\epsilon_F &= (V_- - \bar{V}_{\rm Coul})/\epsilon_F \\ &= F_0'\rho_{{\rm eq},-}/\mathcal{N}_F\epsilon_F - \bar{V}_{\rm Coul}/\epsilon_F, \end{aligned} \tag{B7}$$

where (see Ref. [27])

$$V_- = F_0'\rho_{{\rm eq},-}/\mathcal{N}_F \tag{B8}$$

and the averaged density of states is

$$\mathcal{N}_F = p_F m^*/\pi^2\hbar^3. \tag{B9}$$

Note that the total particle density $\rho_{{\rm eq},+}$ is given (in the linear approximation) by $\rho_{{\rm eq},+} \approx 2p_F^3/3\pi^2\hbar^3 \approx 2\rho_0$. The isovector part of the particle density $\rho_{{\rm eq},-}$ in Eq. (B8) is derived by

$$\rho_{{\rm eq},-} = \left(p_{F,n}^3 - p_{F,p}^3\right)/3\pi^2\hbar^3. \tag{B10}$$

Collecting the kinetic, Eq. (B6), and potential, Eq. (B7), parts of the Fermi energy splitting one obtains (see also Ref. [27])

$$\begin{aligned} 2\Delta = (\epsilon_{F,n} - \epsilon_{F,p})/\epsilon_F &= (\epsilon_{F0,n} - \epsilon_{F0,p} + V_n - V_p)/\epsilon_F \\ &= \frac{4}{3}X\left(1 + F_0' + \frac{3b_{\rm sym}}{\epsilon_F}\right), \end{aligned} \tag{B11}$$

with

$$\epsilon_{F0,n} - \epsilon_{F0,p} = \left[p_{F,n}^2 - p_{F,p}^2\right]/2m^* \approx \tfrac{4}{3}\epsilon_F X. \tag{B12}$$

In the derivation of Eq. (B11), we have used the β-stability condition (B4) and the linearized Eqs. (B10) and (B8) for the first term V_- of the potential part of Eq. (B7),

$$V_- = \tfrac{4}{3}\epsilon_F F_0' X. \tag{B13}$$

Now, we need the expression for the symmetry coefficient $b_{\rm sym}$ in terms of the Landau isovector constant F_0'. For this purpose we recognize that the proton system differs from the neutron one only by the Coulomb interaction, which is the unique source of the difference $\epsilon_{F0,n} - \epsilon_{F0,p}$ and the isovector shift of the mean field V_-; that is,

$$\bar{V}_{\rm Coul} = \epsilon_{F0,n} - \epsilon_{F0,p} + V_-. \tag{B14}$$

Substituting (B5), (B12), and (B13) into (B14) one obtains (see [28])

$$b_{\rm sym} = \tfrac{1}{3}\epsilon_F(1 + F_0'). \tag{B15}$$

Finally, we obtain from Eq. (B11)

$$\Delta = \tfrac{4}{3}X(1 + F_0'). \tag{B16}$$

The Fermi energy splitting Δ has a clear physical meaning as being related to the symmetry coefficient $b_{\rm sym}$ and asymmetry parameter X by

$$\Delta = 4b_{\rm sym}X/\epsilon_F. \tag{B17}$$

APPENDIX C: DISPERSION RELATIONS FOR ASYMMETRIC NUCLEI

For the noncollisional case the dispersion relations for both the symmetric and asymmetric nucleus can be derived from Eq. (20). Using Eq. (23), we rewrite Eq. (20) as

$$\alpha_+^+\Phi_+ + \alpha_+^-\Phi_- = 0, \quad \alpha_-^+\Phi_+ + \alpha_-^-\Phi_- = 0, \tag{C1}$$

where

$$\begin{aligned} \alpha_+^+ &= \frac{F_0}{2}\left[F_0Q_1 - 1 - \Delta F_0'\left(\frac{s^2}{s^2-1} + Q_1\right)\right], \\ \alpha_+^- &= \frac{F_0'}{2}\left[F_0'Q_1 - \frac{F_0}{F_0'} - \Delta F_0\left(\frac{s^2}{s^2-1} + Q_1\right)\right], \\ \alpha_-^+ &= \frac{F_0}{2}\left[F_0Q_1 - 1 + \Delta F_0'\left(\frac{s^2}{s^2-1} + Q_1\right)\right], \\ \alpha_-^- &= \frac{F_0'}{2}\left[\frac{F_0}{F_0'} - F_0'Q_1 - \Delta F_0\left(\frac{s^2}{s^2-1} + Q_1\right)\right]. \end{aligned} \tag{C2}$$

From Eqs. (C1) one obtains the dispersion equation

$$\begin{aligned} \alpha_+^+\alpha_-^- - \alpha_+^-\alpha_-^+ \equiv 4F_0F_0'(F_0Q_1 - 1)(F_0'Q_1 - 1) \\ - \Delta^2F_0^2F_0'^2/4\left(\frac{s^2}{s^2-1} + Q_1\right)^2 = 0. \end{aligned} \tag{C3}$$

The dispersion equation (C3) provides two solutions for the sound velocity: $s = s^{(1)}$ and $s = s^{(2)}$. Using Eqs. (C2), (C3), and (25), for the first solution $s = s^{(1)}$ we find

$$\begin{aligned} \alpha_+^{+(1)} &= -\frac{F_0'(s^{(1)2}(1+F_0)-1)}{2(s^{(1)2}-1)}\Delta, \\ \alpha_+^{-(1)} &= \frac{F_0'}{2F_0}\left[F_0' - F_0 - \frac{F_0(s^{(1)2}(1+F_0)-1)}{s^{(1)2}-1}\Delta\right], \\ \alpha_-^{+(1)} &= \frac{F_0'[s^{(1)2}(1+F_0)-1]}{2(s^{(1)2}-1)}\Delta, \\ \alpha_-^{-(1)} &= \frac{F_0'}{2F_0}\left[F_0 - F_0' - \frac{F_0(s^{(1)2}(1+F_0)-1)}{s^{(1)2}-1}\Delta\right]. \end{aligned} \tag{C4}$$

For the second solution $s = s^{(2)}$ one obtains

$$\begin{aligned} \alpha_+^{+(2)} &= \frac{F_0}{2F_0'}\left[F_0 - F_0' - \frac{F_0'(s^{(2)2}(1+F_0')-1)}{s^{(2)2}-1}\Delta\right], \\ \alpha_+^{-(2)} &= \frac{F_0[1 - s^{(2)2}(1+F_0)]}{2(s^{(2)2}-1)}\Delta, \end{aligned}$$

$$\alpha_-^{+(2)} = \frac{F_0}{2F_0'}\left[F_0' - F_0 - \frac{F_0'[s^{(2)2}(1+F_0')-1]}{s^{(2)2}-1}\Delta\right],$$
$$\alpha_-^{-(2)} = \frac{F_0[1-s^{(2)2}(1+F_0')]}{s^{(2)2}-1}\Delta. \tag{C5}$$

APPENDIX D: VELOCITY FIELD, PRESSURE, AND THE SECULAR EQUATION

The radial components of the velocity field $\mathbf{u}$ and momentum flux tensor $\delta\Pi_{\nu\mu}$ entering the boundary conditions (35) and (36) are obtained from Eqs. (4), (11), (16), and (37) as

$$u_{r,\pm}^{(\kappa)} = \phi_\kappa \bar{u}_{r,\pm}^{(\kappa)}(r) Y_{L0}(\hat{\mathbf{r}}), \qquad \Pi_{rr,\pm}^{(\kappa)} = \phi_\kappa \bar{\Pi}_{rr,\pm}^{(\kappa)}(r) Y_{L0}(\hat{\mathbf{r}}), \tag{D1}$$

where the index κ indicates that we have $s = s^{(\kappa)}$ with $\kappa = 1, 2$, and

$$\begin{aligned}
\bar{u}_{r,+}^{(1)}(r) &= \frac{6i^{L-1}s^{(1)}}{p_F} j_L'(kr),\\
\bar{u}_{r,-}^{(1)}(r) &= \frac{6i^{L-1}s^{(1)}}{p_F}\Delta\left[1+\frac{\Delta_1}{2\Delta}\right] j_L'(kr),\\
\bar{u}_{r,+}^{(2)}(r) &= \frac{6i^{L-1}s^{(2)}}{p_F}\Delta\left[1+\frac{\Delta_2}{2\Delta}\right] j_L'(kr),\\
\bar{u}_{r,-}^{(2)}(r) &= \frac{6i^{L-1}s^{(2)}}{p_F} j_L'(kr)
\end{aligned} \tag{D2}$$

[see also Eqs. (30) and (31) for Δ_1 and Δ_2]. The momentum flux tensor $\bar{\Pi}_{rr}^{(\kappa)}$ is given by

$$\bar{\Pi}_{rr,\pm}^{(\kappa)}(r) = 3\rho_0 i^L\left[a_\pm^{(\kappa)} j_L''(kr) + b_\pm^{(\kappa)} j_L(kr)\right], \tag{D3}$$

where

$$a_+^{(1)} = 1 - 3s^{(1)2} + F_0 + \frac{s^{(1)2}F_0^2}{2(s^{(1)2}-1)}\Delta, \tag{D4}$$

$$\begin{aligned}
b_+^{(1)} &= 1 - s^{(1)2} + F_0 + \frac{s^{(1)2}F_0^2}{6(s^{(1)2}-1)}\Delta,\\
a_-^{(1)} &= \frac{3}{2}\Delta\left[(1-3s^{(1)2}+F_0)\frac{\Delta_1}{3\Delta} - 1 + 2s^{(1)2} - F_0\right],
\end{aligned} \tag{D5}$$

$$\begin{aligned}
b_-^{(1)} = \frac{3}{2}\Delta\Bigg\{&\left[1 - s^{(1)2} + \frac{1}{3}\left(F_0 + 2F_0'\right)\right]\frac{\Delta_1}{3\Delta}\\
&- 1 + \frac{2}{3}s^{(1)2} - F_0\Bigg\},\\
a_+^{(2)} = \frac{3}{2}\Delta&\left[(1-3s^{(2)2}+F_0')\frac{\Delta_2}{3\Delta} - 1 + 2s^{(2)2} - F_0'\right],
\end{aligned} \tag{D6}$$

$$\begin{aligned}
b_+^{(2)} = \frac{3}{2}\Delta\Bigg\{&\left[1 - s_2^2 + \frac{1}{3}\left(F_0' + 2F_0\right)\right]\frac{\Delta_2}{3\Delta}\\
&- 1 + \frac{2}{3}s_2^2 - F_0'\Bigg\}
\end{aligned}$$

$$\begin{aligned}
a_-^{(2)} &= 1 - 3s^{(2)2} + F_0' + \frac{s^{(2)2}F_0'^2}{2(s^{(2)2}-1)}\Delta,\\
b_-^{(2)} &= 1 - s^{(2)2} + F_0' + \frac{s^{(2)2}F_0'^2}{6(s^{(2)2}-1)}\Delta.
\end{aligned} \tag{D7}$$

Equations (D1)–(D7) can be used to reduce the boundary conditions of Eqs. (35) and (36). For the first kind of solutions (IV) [see Eq. (40)], which correspond to the isovector like modes, we finally obtain the following two equations for the $s^{(1)}$ and $s^{(2)}$ solutions of the dispersion equations (25):

$$\begin{aligned}
j_L'(kR_0) &= \frac{3\xi_- kR_0[a_-^{(1)} j_L''(kR_0) + b_-^{(1)} j_L(kR_0)]}{4(\Delta + \Delta_1/2)},\\
&\qquad \text{for } s = s^{(1)},\\
j_L'(kR_0) &= \tfrac{3}{2}\xi_- kR_0[a_-^{(2)} j_L''(kR_0) + b_-^{(2)} j_L(kR_0)],\\
&\qquad \text{for } s = s^{(2)},
\end{aligned} \tag{D8}$$

where $\xi_- = \epsilon_F/b_{s,-}A^{1/3}$. For other solutions, which correspond to the isoscalar modes (IS), one obtains, respectively,

$$\begin{aligned}
j_L'(kR_0) &= \frac{3\xi_+ kR_0[a_+^{(1)} j_L''(kR_0) + b_+^{(1)} j_L(kR_0)]}{(L-1)(L+2)},\\
&\qquad \text{for } s = s^{(1)},\\
j_L'(kR_0) &= \frac{3\xi_+ kR_0[a_+^{(2)} j_L''(kR_0) + b_+^{(2)} j_L(kR_0)]}{(L-1)(L+2)(\Delta + \Delta_2/2)},\\
&\qquad \text{for } s = s^{(2)},
\end{aligned} \tag{D9}$$

where $\xi_+ = \epsilon_F A^{1/3}/b_{s,+}$ and $L \neq 1$. The surface energy constants $b_{s,\pm}$ are defined in Appendix E.

For the isovector modes (IV) for which we present numerical results in this work we rewrite the characteristic equations (D8) in the more transparent form of Eqs. (42) and (43), where

$$\begin{aligned}
\mathcal{C}_1^{(1)} &= \{\mathcal{R}[1 - F_0'(3s^{(1)2}/Q_1 - 1)] + (Q_1 - F_0')\\
&\quad \times[3s^{(1)2}(Q_1 - \mathcal{K}) + [3s^{(1)2}F_0/Q_1 - 3(Q_1+1)\\
&\quad + Q_1 - F_0]\mathcal{K}]\}/\mathcal{C},\\
\mathcal{C}_2^{(1)} &= \{\mathcal{R}[1 - F_0'(s^{(1)2}/Q_1 + 1/3)] + (Q_1 - F_0')\\
&\quad \times[s^{(1)2}(Q_1 - \mathcal{K}) - [2F_0 s^{(1)2}/Q_1 + 3(Q_1/3 - \mathcal{K})\\
&\quad + (Q_1 - F_0)(3s^{(1)2}/Q_1 - 1/3) - 2F_0]\mathcal{K}]\}/\mathcal{C},\\
\mathcal{C}_1^{(2)} &= 1 - 3s^{(2)2} + F_0', \qquad \mathcal{C}_2^{(2)} = 1 - s^{(2)2} + F_0',
\end{aligned} \tag{D10}$$

where $\mathcal{K} = s^{(1)2} - 1$ and

$$\begin{aligned}
\mathcal{C} &= G_1\{F_0'\mathcal{R} + [Q_1\mathcal{K}(1 + 1/G_1) + \mathcal{R}](Q_1 - F_0')\}/Q_1,\\
\mathcal{R} &= (2Q_1 - F_0)\mathcal{K} - Q_1^2.
\end{aligned} \tag{D11}$$

APPENDIX E: BOUNDARY CONDITIONS FOR ASYMMETRIC NUCLEI

1. Boundary condition for the velocity field

We will start from the continuity equation (A8) and transform all functions and derivatives of the Cartesian coordinates $\mathbf{r}$ in Eq. (A8) to the cylindrical ones $\{\rho, z, \varphi\}$ for the axially

symmetric surface shapes. By making use of the coordinate system $\{\xi, \eta\}$ related to the moving surface in the plane of the symmetry axis z (with ξ the normal-to-surface coordinate and η perpendicular to the surface) and then integrating over ξ from ∞ to some point $\xi_{\rm in}$ inside the Fermion system, we get [33–35]

$$\int_{\infty}^{\xi_{\rm in}} d\xi \left[\frac{\partial}{\partial t}\rho_{\pm}(\xi,\eta,t) + \dot{\xi}\frac{\partial \rho_{\pm}}{\partial \xi} + \dot{\eta}\frac{\partial \rho_{\pm}}{\partial \eta} + \frac{\partial j_{\xi,\pm}}{\partial \xi} + \frac{\partial j_{\eta,\pm}}{\partial \eta}\right] = 0, \tag{E1}$$

where $\mathbf{j}_q(\mathbf{r},t) = \rho_q(\mathbf{r},t)\mathbf{u}_q(\mathbf{r},t)$ is the current density and $\mathbf{j}_{\pm} = \mathbf{j}_p \pm \mathbf{j}_n$. The integral in Eq. (E1) converges within a small region of the order of the diffuseness parameter a of the nuclear surface. With the precision of the effective surface approximation (ESA) of [33], up to higher order terms in the expansion in the parameter $a/R_0 \approx A^{-1/3}$, one approximately obtains

$$\int_{\infty}^{\xi_{in}} d\xi \left[\frac{\partial \rho_{\rm eq,\pm}}{\partial \xi}\left(-u_{s,\pm} + \frac{\partial u_{\xi,\pm}}{\partial \xi}\right)\right] = 0, \tag{E2}$$

where

$$\dot{\xi} = u_{s,\pm}. \tag{E3}$$

We took into account here that only the derivatives of the density and current in the normal direction to the surface give the main contributions to the integrand in Eq. (E2). Taking smooth quantities in Eqs. (E2) off the integral at the surface, defined as the positions of maximal gradient of the particle density $\rho_{\rm eq,\pm}$, and integrating the remaining derivatives over ξ, one finally obtains the first boundary condition (35).

2. *Boundary condition for the momentum flux tensor*

For the derivation of the second boundary condition we use also the ESA method starting from the momentum conservation equations

$$m_q \frac{\partial}{\partial t} j_{v,q} + \sum_{\mu} \frac{\partial}{\partial r_{\mu}} \Pi_{v\mu,q} = 0. \tag{E4}$$

Following [34,35], we need to specify only the energy density functional $\mathcal{E}(\rho_p, \rho_n)$ for the asymmetric Fermi-liquid drop,

$$\mathcal{E}(\rho_p,\rho_n) = \mathcal{A}(\rho_p,\rho_n) + \mathcal{B}_{pp}(\nabla\rho_p)^2 + 2\mathcal{B}_{pn}\nabla\rho_p\nabla\rho_n + \mathcal{B}_{nn}(\nabla\rho_n)^2, \tag{E5}$$

where $\mathcal{A}$ and $\mathcal{B}_{qq'}$ are smooth functions of the particle densities ρ_q. The energy density functional $\mathcal{E}(\rho_p, \rho_n)$ can be identically written as

$$\mathcal{E}(\rho_p,\rho_n) \equiv \mathcal{E}(\rho_+,\rho_-) = \mathcal{A}(\rho_+,\rho_-) + \mathcal{B}_+^+(\nabla\rho_+)^2 + 2\mathcal{B}_+^-\nabla\rho_+\nabla\rho_- + \mathcal{B}_-^-(\nabla\rho_-)^2, \tag{E6}$$

with the obvious relations between the new, $\mathcal{B}_{\pm}^{\pm}$, and the old, $\mathcal{B}_{qq'}$, smooth functions. According to Refs. [32–34], we derive the basic expressions

$$\rho_0\left(\frac{\delta\mathcal{E}}{\delta\rho_+}\right)_s = -b_{V,+} + 2\sigma_+^+\mathcal{H}_+ + 2\sigma_+^-\mathcal{H}_-,$$
$$\rho_0\left(\frac{\delta\mathcal{E}}{\delta\rho_-}\right)_s = -b_{V,-} + 2\sigma_-^+\mathcal{H}_+ + 2\sigma_-^-\mathcal{H}_-, \tag{E7}$$

where $b_{V,\pm}$ are constants,

$$\sigma_+^+ = 2\mathcal{B}_+^+\int_{-\infty}^{\infty} d\xi \left(\frac{\partial\rho_{\rm eq,+}}{\partial\xi}\right)^2,$$
$$\sigma_-^- = 2\mathcal{B}_-^-\int_{-\infty}^{\infty} d\xi \left(\frac{\partial\rho_{\rm eq,-}}{\partial\xi}\right)^2, \tag{E8}$$
$$\sigma_+^- = \sigma_-^+ = 2\mathcal{B}_+^-\int_{-\infty}^{\infty} d\xi \frac{\partial\rho_{\rm eq,+}}{\partial\xi}\frac{\partial\rho_{\rm eq,-}}{\partial\xi}$$

are the matrix elements of the surface tension, and $\mathcal{H}_{\pm}$ are the mean Gaussian "curvatures" related to the isoscalar and isovector motions of the surface (see Ref. [33]). The surface tension pressures $\delta\mathcal{P}_{s,\pm}$ are determined by the surface tension coefficients $\sigma_{\pm}^{\pm}$. Namely,

$$\delta\mathcal{P}_{s,+} = \delta\mathcal{P}_{s,+}^+ + \delta\mathcal{P}_{s,+}^-, \quad \delta\mathcal{P}_{s,-} = \delta\mathcal{P}_{s,-}^+ + \delta\mathcal{P}_{s,-}^-, \tag{E9}$$

where

$$\delta\mathcal{P}_{s,+}^+ = 2\sigma_+^+\delta\mathcal{H}_+ = \alpha_{s,+}\rho_0 b_{s,+}/[3A^{1/3}(L-1)(L+2)],$$
$$\delta\mathcal{P}_{s,-}^- = 2\sigma_-^-\delta\mathcal{H}_- = 2\alpha_{s,-}\rho_0 b_{s,-}A^{1/3}/3, \tag{E10}$$
$$\delta\mathcal{P}_{s,+}^- = 2\sigma_+^-\delta\mathcal{H}_-, \qquad \delta\mathcal{P}_{s,-}^+ = 2\sigma_-^+\delta\mathcal{H}_+.$$

The explicit expressions for the variation of the "curvature" $\delta\mathcal{H}_{\pm}$ can be determined from Eqs. (E6), (E7), and (E8). We also point out that in Eq. (36) of Sec. II we have introduced the reduced surface pressure $\bar{\mathcal{P}}_{s,\pm}$ by the relation $\delta\mathcal{P}_{s,\pm} = \alpha_{s,\pm}\bar{\mathcal{P}}_s^{\pm}$, where $\alpha_{s,\pm} = \alpha_{s,p} \pm \alpha_{s,n}$ and the vibration amplitude $\alpha_{s,q}$ is derived by $R_q(t) = R_0[1 + \alpha_{s,q}(t)Y_{L0}(\hat{\mathbf{r}})]$.

Note that the boundary condition (36) does not violate the condition of conservation of total momentum $\mathbf{K}$ of the nucleus. In the derivation of the boundary condition (36) we have used the self-consistency relation associated with the translation invariance condition (see [27]). The self-consistency relation reads [34,35]

$$\delta\rho_q\frac{\partial V_q}{\partial r_{\mu}} - \delta V_q\frac{\partial\rho_q}{\partial r_{\mu}} = 0. \tag{E11}$$

The total momentum $\mathbf{K}$ of the nucleus is given by

$$\mathbf{K} = m\sum_q \int d\mathbf{r}\,\mathbf{j}_q(\mathbf{r},t) = mA\dot{\mathbf{R}}_{\rm c.m.}, \tag{E12}$$

where $\mathbf{R}_{\rm c.m.}$ is the radius vector of the nuclear center of mass. Using the momentum conservation equation (E4) and the ESA approach of Ref. [30], one can obtain

$$\frac{\partial K_{\mu}}{\partial t} = -\sum_q \int d\mathbf{r}\left(\delta\rho_q\frac{\partial V_q}{\partial r_{\mu}} - \delta V_q\frac{\partial\rho_q}{\partial r_{\mu}}\right). \tag{E13}$$

The self-consistency relations of Eqs. (E11) and (E13) provide the condition of total momentum conservation:

$$\frac{\partial K_{\mu}}{\partial t} = 0. \tag{E14}$$

As mentioned in the main text [see the discussion after Eq. (53)] the dynamical variation $\delta\mathbf{R}_{\rm c.m.}$ of the center of mass $\mathbf{R}_{\rm c.m.}$ in the laboratory coordinate system is identically zero

owing to the transition density $\delta\rho_q(\mathbf{r}, t)$ taken in the form of Eq. (53). Hence, momentum conservation (E14) does not lead to a spurious state mixing (associated with the c.m. motion) because of the relations (E12) and (56).

[1] V. S. Ishkanov and I. M. Kapitonov, *Electromagnetic Radiation Interaction with Nuclei* (Moscow State University, Moscow, 1970) (in Russian).

[2] B. L. Berman and S. C. Fultz, Rev. Mod. Phys. **47**, 713 (1975).

[3] S. Oifawa and K. Shoda, Nucl. Phys. **A277**, 301 (1977).

[4] J. G. Woodworth, K. G. McNeill, J. W. Jury, R. A. Alvarez, B. L. Berman, D. D. Faul, and P. Meyer, Phys. Rev. C **19**, 1667 (1979).

[5] Y. I. Assafiri and M. N. Thompson, Nucl. Phys. **A357**, 429 (1981).

[6] P. D. Harty and M. N. Thompson, Aust. J. Phys. **34**, 505 (1981).

[7] K. Itoh, Y. M. Shin, T. Saito, and Y. Torizuka, Phys. Rev. C **24**, 1969 (1981).

[8] S. C. Fultz, R. A. Alvarez, B. L. Berman, and P. Meyer, Phys. Rev. C **10**, 608 (1974).

[9] I. Bergqvist, in *Neutron Radiative Capture*, edited by R. E. Chrien (Pergamon, Oxford, 1984), Vol. 3, p. 33.

[10] R. E. Pywell, B. L. Berman, J. G. Woodworth, J. G. Jury, K. G. McNeill, and M. N. Thompson, Phys. Rev. C **32**, 384 (1985).

[11] G. J. O'Keefe, M. N. Thompson, Y. I. Assafiri, R. E. Pywell, and K. Shoda, Nucl. Phys. **A469**, 239 (1987).

[12] A. Van der Woude, Prog. Part. Nucl. Phys. **18**, 217 (1987).

[13] B. Goulard and S. Fallieros, Can. J. Phys. **45**, 3221 (1967).

[14] R. Ö. Akyüz and S. Fallieros, Phys. Rev. Lett. **27**, 1016 (1971).

[15] P. Carlos, *et al*., Nucl. Phys. **A225**, 171 (1974).

[16] J. M. Eisenberg and W. Greiner, *Nuclear Models* (North-Holland, Amsterdam, 1970), Vol. 1.

[17] A. Bohr and B. R. Mottelson, *Nuclear Structure* (Benjamin, New York, 1975), Vol. II.

[18] E. Lipparini and S. Stringari, Phys. Rev. C **36**, 2697 (1987).

[19] I. Hamamoto, H. Sagawa, and X. Z. Zhang, Phys. Rev. C **55**, 2361 (1997); **56**, 3121 (1997); **57**, R1064 (1998); Nucl. Phys. **A648**, 203 (1999).

[20] I. Hamamoto, Phys. Rev. C **60**, 031303(R) (1999).

[21] V. M. Kolomietz, A. G. Magner, and V. A. Plujko, Z. Phys. A **345**, 131 (1993).

[22] A G. Magner, V. M. Kolomietz, H. Hofmann, and S. Shlomo, Phys. Rev. C **51**, 2457 (1995).

[23] V. M. Kolomietz and S. Shlomo, Phys. Rep. **390**, 133 (2004).

[24] A. A. Abrikosov and I. M. Khalatnikov, Rep. Prog. Phys. **22**, 329 (1959).

[25] V. M. Kolomietz, *Local Density Approximation in Atomic and Nuclear Physics* (Naukova Dumka, Kiev, 1990) (in Russian).

[26] V. A. Khodel and E. E. Saperstein, Phys. Rep. **92**, 183 (1982).

[27] A. B. Migdal, *The Finite Fermi-System Theory and Atomic Nuclear Properties* (Nauka, Moscow, 1983) (in Russian).

[28] D. F. Zaretsky and M. G. Urin, Sov. Phys. JETP Lett. **4**, 255 (1966).

[29] V. M. Kolomietz, A. B. Larionov, and M. Di Toro, Nucl. Phys. **A613**, 1 (1997).

[30] A. G. Magner, V. Y. Denisov, Sov. J. Nucl. Phys. **46**, 604 (1987) [Yad. Fiz. **46**, 1047 (1987)].

[31] S. Shlomo, V. M. Kolomietz, and B. K. Agrawal, Phys. Rev. C **68**, 064301 (2003).

[32] V. M. Strutinsky, A. G. Magner, and V. Yu. Denisov, Z. Phys. A **322**, 149 (1985).

[33] V. M. Strutinsky, A. G. Magner and M. Brack, Z. Phys. A **319**, 205 (1984).

[34] A. G. Magner and V. M. Strutinsky, Z. Phys. A **322**, 633 (1985); Sov. J. Nucl. Phys. **44**, 591 (1986).

[35] A. G. Magner, Sov. J. Nucl. Phys. **45**, 235 (1987) [Yad. Fiz. **45**, 374 (1987)].

[36] E. Lipparini and S. Stringari, Phys. Rep. **175**, 103 (1989).

[37] V. V. Varlamov, V. V. Sapunenko, and M. E. Stepanov, *Photonuclear Data 1976–1995* (Moscow State University, Moscow, 1996), pp. 1–220 (http://cdfe.sinp.msu.ru/services/index.html).

[38] V. V. Varlamov, B. S. Ishkanov, and M. E. Stepanov, *Systematics of Main Parameters of Atomic Nuclei Giant Dipole Resonances and Photonuclear Reaction Threshold Values* (Moscow State University, Institute of Nuclear Physics, Preprint-96-32/439, Moscow, 1996).

[39] S. S. Dietrich and B. L. Berman, At. Data Nucl. Data Tables **38**, 199 (1988).

[40] H. Heiselberg, C. J. Pethick, and D. G. Ravenhall, Ann. Phys. (NY) **223**, 37 (1993).

[41] R. Balescu, *Equilibrium and Nonequilibrium Statistical Mechanics* (Wiley, New York, London, 1975), Vol. II.